AN ANALYSIS OF SPRAY DEVELOPMENT WITH ISO-OCTANE, N-PENTANE, GASOLINE, ETHANOL AND N-BUTANOL FROM A MULTI-HOLE INJECTOR UNDER HOT FUEL CONDITIONS

P.G. Aleiferis* and Z.R. van Romunde

Department of Mechanical Engineering, University College London, UK

*Author for Correspondence:

Dr. Pavlos Aleiferis

University College London

Department of Mechanical Engineering

Torrington Place, London WC1E 7JE, UK

Tel: +44-(0)20-76793862, Fax: +44-(0)20-73880180

E-mail: p.aleiferis@ucl.ac.uk

Full length article accepted for publication in Fuel.

ABSTRACT

High-pressure multi-hole injectors for direct-injection spark-ignition engines offer some great benefits in terms of fuel atomisation, as well as flexibility in fuel targeting by selection of the number and angle of the nozzle's holes. However, very few data exist for injector-body temperatures representative of engine operation with various fuels, especially at low-load conditions with early injection strategies that can also lead to phase change due to fuel flash boiling upon injection. The challenge is further complicated by the predicted fuel stocks which will include a significant bio-derived component presenting the requirement to manage fuel flexibility. The physical/chemical properties of bio-components, like various types of alcohols, can differ markedly from gasoline and it is important to study their effects in direct comparison to liquid hydrocarbons. This work outlines results from an optical investigation (high-speed imaging and droplet sizing) into the effects of fuel properties, temperature and pressure conditions on the extent of spray formation. Specifically, gasoline, *iso*-octane, *n*-pentane, ethanol and *n*-butanol were tested at 20, 50, 90 and 120 °C injector body temperatures for ambient pressures of 0.5 bar and 1.0 bar in order to simulate early homogeneous injection strategies for part-load and wide open throttle engine operation; some test were also carried out at 180 °C, 0.3 bar. Droplet sizing was also performed for gasoline, *iso*-octane and *n*-pentane using Phase Doppler and Laser Diffraction techniques in order to understand the effects of low- and high-volatility components on the atomization of the multi-component gasoline. The boiling points and distillation curves of all fuels, their vapour pressures and bubble points, as well as density, viscosity and surface tension were obtained and the Reynolds, Weber and Ohnesorge numbers were considered in the analysis.

NOMENCLATURE

d	Diameter
μ	Dynamic Viscosity
Oh	Ohnesorghe Number
ρ	Density
Re	Reynolds Number
σ	Surface Tension
u	Velocity
We	Weber Number

ABBREVIATIONS

ASOI	After Start Of Injection
ASTM	American Society for Testing and Materials
DISI	Direct Injection Spark Ignition
DVPE	Dry Vapour Pressure Equivalent
EOI	End Of Injection
MON	Motor Octane Number
RON	Research Octane Number
RPM	Revolutions Per Minute
SMD	Sauter Mean Diameter
SOI	Start Of Injection

INTRODUCTION

INJECTION SYSTEMS FOR DIRECT-INJECTION SPARK-IGNITION ENGINES

The gasoline Direct-Injection Spark-Ignition (DISI) engine has several practical advantages over the port-fuel injected engine, such as greater precision in fuel metering and significant potential in fuel economy benefits. Other advantages, such as larger charge cooling potential, allow higher engine compression ratios to be used, increasing the thermal efficiency. However over the last 10 years it has become clear that the successful implementation of all these benefits has been more difficult to achieve than previously expected. The main reason has been the inadequate performance of some direct-injection systems, as well as the engine calibration strategies used, which have not delivered the level of improvements in power, fuel economy and emissions promised by manufacturers. For example, first generation side-injection systems relied on a piston-bowl to achieve the 'stratified charge' concept, but were plagued by pool fires on the piston as the fuel failed to evaporate fully in the time available before ignition, thus producing unacceptable levels of particulate emissions and unburned hydrocarbons [1]. Latest design high-pressure multi-hole injectors located in close spacing arrangement with the spark plug aim to resolve these issues by providing accurate spray directionality through a number of nozzle holes which can be designed to target the fuel delivery where necessary, *e.g.* towards the spark plug or any other in-cylinder area of interest, and by flexibility of when and how fuel is injected into the cylinder *i.e.* independence over piston position [2–4].

The majority of work published to date on multi-hole injectors concerns Diesel nozzle geometries, with particular experimental features and analysis targeted at this combustion system. The sensitivities to geometrical differences of the injector nozzles and piston design, the varied operating conditions for the DISI combustion system and its particular mixture preparation requirements merit specific attention and are the motives behind continued research in this field. For example, DISI injectors are mounted in the engine head where the fuel inside the injector and the spray upon injection are both subjected to a wide range of temperature and pressure. More specifically, DISI injectors must inject fuel at conditions of low in-cylinder pressure, typically from ~0.2 bar at low load with early injection strategies for homogeneous mixture formation, to ~5 bar for late-injection strategies under stratified engine operation, or even more under supercharged operation. Additionally, fuel temperatures can vary from below 0 °C at cold-start engine conditions to over 150 °C at the injector tip under high-load firing conditions. Although quite significant phenomena are coupled over this operation regime, very few experimental results exist to explain such effects from multi-hole injectors for DISI engines. For example, at low-load operation with fully-warm engine, fuel 'flash-boiling' can occur from fast disruptive evaporation upon injection due to the reduction of the fuel's boiling temperature from rapid depressurisation into the sub-atmospheric engine cylinder. This enhances the rate of evaporation but also leads to 'spray collapse' that draws the plumes close together under the injector tip and destroys the designed directionality of the spray.

ALTERNATIVE FUELS FOR SPARK-IGNITION ENGINES

Global concerns over the use of fossil fuels are leading to an increased demand for biogenically derived fuels. Hence, the challenge for combustion system engineers is further complicated by the predicted fuel stocks which will include a significant bio-derived component in order to strengthen sustainability and reduce CO_2 emissions, presenting the immediate requirement to manage fuel flexibility. Understanding the effect of new

bio-components on fundamental engine processes, such as spray formation, is an essential part of the challenges involved, especially in DISI engines that are quite sensitive to fuel properties.

The production of such bio-components is done primarily by fermentation of glucose and cellulose, resulting in alcohols. The higher activation energy of alcohols leads to increased octane number, hence better resistance to engine knock that can allow higher compression ratios and greater engine thermal efficiencies. In addition, their higher heat of vaporisation of alcohols leads to charge cooling effects, increasing the charge's density and further the thermodynamic efficiency. Gasoline already contains 5% bio-ethanol (E5) in many countries (*e.g.* the UK), or 10% in others (*e.g.* Germany), and is compatible with existing combustion systems but its use will have only limited impact on CO_2 emissions. Therefore, there is pressure for the ethanol content of fuels to increase with some markets demanding much higher proportions (E85 or E100). However, at high Ethanol content blends issues may arise at cold-start engine conditions due to lack of fuel volatility. Additionally, the chemistry of ethanol is very different from that of hydrocarbons; for one thing Ethanol is water soluble which necessitates rigorous procedures during fuel distribution and secondly not all components/materials on the vehicle are necessarily compatible with Ethanol. The volumetric energy density of Ethanol is also lower than Gasoline which poses further challenges for the engine calibrator in terms of controlling the injector pulse width. Other alkyl alcohols have also been suggested as possible Gasoline bio-components and recent studies have focused on their fundamental combustion properties. A typical example of this kind is Butanol [5]. The longer hydrocarbon chain of Butanol makes it relatively non-polar and less miscible in water. Butanol also has an energy content and heat of vaporisation more akin to Gasoline's, but on the other hand it has a higher surface tension and boiling point than most typical fuels, suggesting quite different atomization and in-cylinder mixture preparation processes. Butanol also lags behind Ethanol in terms of commercial production. With regards to other alcohols, it may be noted that the demand and cost for Propanol is driven mainly by its use as a solvent and that currently it is not commonly considered as a future fuel. However, some studies have started to emerge recently on the fundamental combustion properties of Propanol and its isomers [6, 7].

PRESENT CONTRIBUTION

Because of the ability of multi-hole injectors to target fuel directly to specific areas inside the cylinder for robust mixture formation, it is important to understand whether strict criteria are maintained when fuels other than those used to test the injectors at design and optimisation stage are employed in real engines. Specifically, there is limited understanding about the role that liquid transport properties such as surface tension, viscosity, density, boiling point and vapour pressure have on overall spray development, and how these are affected by the wide operating envelope of DISI engine injectors. There are also very limited experimental results of the interactions between flash-boiling and spray formation at extremes of pressure and temperature with various types of fuels, especially bio-derived. Therefore, the main objective of this work was to investigate such effects using a latest design multi-hole injector. Specifically, the current paper presents imaging of the spray's formation and subsequently quantification of spray properties, like spray tip penetration and velocity, as well as cone angles. Tests were carried out in a quiescent pressure chamber with five different fuels, namely a standard commercial grade Gasoline (RON 95), *iso*-Octane, *n*-Pentane and *iso*-Octane, Ethanol and Butanol over a range of atmospheric and sub-atmospheric gas pressures at 20–180 °C injector temperatures. Droplet sizing was also performed in an attempt to link the spray formation of the multi-component Gasoline to its low and mid-

volatility components *n*-Pentane and *iso*-Octane. The work is believed to contribute towards a comprehensive database of spray development data which are essential for developing our knowledge of the underlying mechanisms responsible for atomisation under realistic engine conditions. Such a database is also useful to spray modellers because accurate simulation of spray break-up mechanisms from first principles is very challenging; only models of limited applicability currently exist at high fuel temperature and low gas pressure conditions where significant alteration of the spray's nominal pattern can occur. The discussion also makes an attempt to link non-dimensional numbers from atomisation theory to measurements and observations of a practical injection system with latest nozzle geometry using various fuels. To the best of our knowledge, currently there is no other major optical study in the literature discussing spray formation phenomena with all those fuels from a multi-hole injector under such a range of conditions.

EXPERIMENT APPARATUS AND PROCEDURE

INJECTOR

A multi-hole injector designed for vertical installation in close spacing arrangement with the spark plug of a DISI engine was used. The injector had six nozzle holes in an asymmetric arrangement with different angles with respect to the vertical axis. **Fig. 1** shows a schematic of the injector and its spray plumes through two views. Plumes 1 and 6 had a 58.5° inclination with respect to the vertical axis and have been designed to pass on either sides of the spark plug *i.e.* one at the intake side and the other at the exhaust side of the engine. More details about the injector geometry, nozzle-hole angles and spray formation in a quiescent environment and in a running DISI engine can be found in previous studies by the current authors [3, 4, 8–10].

FUELS

Five fuels were investigated: a typical commercial grade Gasoline (RON95), Ethanol, *n*-Butanol, *iso*-Octane and *n*-Pentane[†]. The distillation curve of the Gasoline fuel, as well as the boiling points of the single-component fuels, are all illustrated in **Fig. 2**. A commercial grade European gasoline contains several hydrocarbons typically about 35–40% C5 or lower (including oxygenates), similar levels of C6–C8 and the remainder C9–C10 hydrocarbon chains. *Iso*-Octane is a single component of Gasoline with boiling point temperature of 99 °C at atmospheric pressure, while *n*-Pentane, also a single component of Gasoline, boils at 36.1 °C. Ethanol boils at 78.4 °C and *n*-Butanol at 117 °C at atmospheric pressure. It should be noted here that *n*-Butanol (1-Butanol) was selected for this study instead of its isomer *iso*-Butanol because of the existence of some data on laminar burning velocity for this fuel that could assist parallel analysis of engine combustion data in direct comparison to the other fuels [11–13]. However, *iso*-Butanol is currently also being studied and results will be discussed in future publications (some laminar burning velocity data for Butanol's isomers have also been recently published [14]). Finally *o*-xylene, a heavier component of Gasoline with boiling temperature 144 °C (and octane rating closer to that of Gasoline's than other Xylene isomers) was also considered in the analysis of the current study and has been included in **Fig. 2**, as well as in subsequent various plots to aid results discussions, but was not included in the test matrix because its properties made it quite insensitive to flash-boiling phenomena. Therefore, this component serves only to define the range of Gasoline's thermo-physical properties, which is useful when discussing the effects of Gasoline as a multi-component fuel.

[†] The fuel names have been capitalised throughout this paper for better clarity.

Some typical properties of the fuels used are summarised in **Table 1**. The vapour pressure curves of the fuels are shown in **Fig. 3**. The vapour pressures for the single-component hydrocarbons and alcohols were calculated using correlations obtained from [15] within a valid temperature range. For Gasoline the vapour pressures were obtained experimentally using ASTM D5190 (Dry Vapour Pressure Equivalent, DVPE) at Shell Global Solutions (UK), Ltd. Bubble point and dew point pressures were also calculated at various temperatures, also shown in **Fig. 3**, using a Redlich-Kwong equation of state based on UNIFAC method coefficients for each species identified on the gas chromatograph. The bubble point of a liquid refers to the pressure, below which bubbles will form at the given temperature. Likewise the dew point is the pressure below which the fluid is in vapour state at the given temperature. An increase in pressure over the dew point leads to the formation of liquid droplets at this temperature. Clearly the bubble and dew point pressures are the same for single-component fuels. The bubble point is likely to be indicative of conditions under which light ends begin to flash off in a fuel spray, whereas the dew point may be loosely indicative of the final evaporation of heavy ends from a droplet. It should be noted, however, that the bubble point and dew point are based on equilibrium concepts and during a transient process, like that of injection, heat and mass transfer effects complicate the picture. Nevertheless, their influence is significant for fuel spray evaporation in engines and cross-analysis with acquired spray data is interesting and important.

INJECTION CHAMBER

All fuel injection events were conducted in a quiescent pressure chamber [9, 10]. Its octagonal shape and its six optical windows enable simultaneous multi-technique characterisation such as imaging with back lighting or side lighting, and the use of on-axis and off-axis techniques for droplet sizing and velocity measurements (Phase Doppler and Malvern). The chamber's gas pressure (*i.e.* the injector's 'back' pressure) was monitored by an absolute pressure sensor mounted in the lid of the chamber. The chamber's gas temperature was monitored throughout the experiment by a K-type thermocouple mounted in the lid of the chamber with the sensing tip located near the injector mounting. A valve at the bottom of the pressure chamber enabled evacuation of liquid and vapour fuel as well as creating sub-atmospheric pressure within the chamber through its connection to a vacuum pump system.

The injector was fitted into a specially designed mount positioned at the centre of the upper lid of the pressure chamber. A band heater was attached to the injector to heat up its body temperature, replicating *in-situ* heating of injectors mounted in DISI engine heads. A thermocouple sensor provided feedback to a temperature controller which regulated the injector temperature as required by each experiment. The temperature measured was that of the injector body, as this was the best possible arrangement in obtaining the fuel temperature using the available apparatus. As a result of this, each time the system was heated to a particular test temperature and the temperature was held constant for an hour, allowing enough heat-soak for a uniform distribution of temperature within the whole injector mount mass, before spray imaging was conducted. Therefore, in this paper, the term 'injector-body temperature' corresponds to the temperature reading of this thermocouple, *i.e.*, the temperature of the injector as close to the injector tip as possible.

TEST CONDITIONS

The fuel injection pressure was supplied by a pneumatic-piston ram pump at 150 bar. Just before the injector, there were a bleed valve, a pressure gauge and a safety valve. To mimic the conditions of the injector body

when mounted in an engine, the injector body mounting was heated to temperatures of 20, 50, 90 and 120 °C. In-cylinder engine gas pressures at time of injection were replicated by inducing a vacuum (0.5 bar absolute for early injection strategies at part-load 'homogeneous' charge operation). Tests were also carried out at atmospheric pressure (nominally 1.0 bar). Injection duration was held constant at 1.5 ms pulse-width for all conditions, with the camera recording for 2.5 ms each injection to capture initial, steady-state, end of injection and post injection spray characteristics. Due to obscuration of the spray tips by the pressure chamber windows, it was only possible to measure spray tip penetrations until approximately 1.0 ms After the Start Of Injection (ASOI, *i.e.* the time period following the rising edge of the trigger pulse sent to the injector driver unit). The average driver delay from the start of the injection pulse (Start of Injection, SOI) to fuel seen at the injector tip was of the order 300 μs, as has been quantified in detail in [8].

SPRAY VISUALIZATION SETUP

The injector was mounted at 19° to the vertical in order to optimise the imaging arrangement. The spray was recorded at a frame rate of 9,000 frames per second, equivalent to one spray image at each Crank Angle degree (°CA) for an engine running at 1500 RPM. The camera allowed a maximum spatial resolution of 640×480 pixels at this frame rate (160 μm/pixel). The shutter was set to 1 μs. Illumination was achieved with backlighting using a Multiblitz Variolite 500 photographic spark flash of 4 ms duration diffused through a semi opaque Perspex sheet. The image was a shadowgraph of the spray, therefore only the liquid phase was visualised with this technique. As a result of the back illumination method and the geometry of the injector, each imaged spray plume was essentially the superposition of two plumes (see *z-y* view in **Fig. 1**). Camera shutter speed was set to 1/50,000 s to allow several 'frozen' images to be acquired over the flash duration. Triggering of the high speed camera, flash lamp and solenoid valve was provided by an AVL 327 engine timing unit. 200 injection events and an average background image were captured. The background image for each time interval in the imaging sequence was removed from the spray images to account for differences in lighting over each run. Each corrected image was then thresholded at a value based on the mean of background pixels to leave a binary image. The image was then rotated to align each plume pair with the vertical axis and each plume pair was 'scanned' to find the plume tip. The distance from the plume tip to the nozzle was scaled to calculate a plume pair length. To determine the optimum threshold for automated processing, detailed sensitivity analysis was carried out on the penetration based on different threshold levels and the uncertainty in the calculated values was found to be better than 4% [16].

High magnification imaging of the spray close to the nozzle's exit was also conducted with the same flash and camera equipment but with a Model K2/SC series long-distance microscope system from INFINITY. In order to capture the first fuel seen from the injector nozzle and the ensuing spray development, the frame rate of the high speed camera for the latter was increased to 50 kHz, giving a time period between frames of 20 μs. In order to allow adequate light intensity to be captured for the shadowgraphs, the image integration period (shutter speed) was over the duration of each image; *i.e.* 20 μs. Due to the fixed processing capacity of the camera, increasing the frame rate decreased its resolution to 256 by 128 pixels. Additionally, some tests were performed close to the nozzle with high intensity Laser illumination. The source light from a Nd:YAG Laser (New Wave Pegasus) was passed through a sheet forming lens to form a vertical light sheet, which was aligned to plume 1. For these images, the laser was synchronised to the camera so as to provide a light pulse at the same

frequency and timing as the camera shutter opening. The camera was operated again at a frame rate of 50 kHz, allowing the initial spray as well as the end of injection droplets, to be captured as they passed through the illuminating laser light sheet. Due to the angular projection of the plumes and the fixed alignment of the sheet, it was only possible to visualise a small section of the spray at the nozzle orifice before the liquid spray in front of the sheet obscured the illuminated section of the plume.

DROPLET SIZING

Droplet sizing of the spray was carried out using a TSI Phase Doppler Anemometry system. The Phase Doppler technique is well established and details on its principles can be found in [17]. The system consisting of a Coherent Innova 70C Argon-Ion laser (5 W) coupled to a TSI beam splitter and Bragg cell. Both the transmitter and receiver had an optical focal length of 250 mm. The forward scattering angle was set to 40°. Droplet measurements were recorded 25 mm downstream from the injector tip, along the chamber's central axis. Measurements were taken in the centre of plume 2, which was the central plume nearest the camera. To compensate for alterations in the spray's global form at high-temperature/low-pressure conditions and hence to ensure that the droplets at the same axial radius were measured for all conditions, the location of the PDA measurement region was altered for each condition in line with the expected degree of plume convergence recorded by imaging; for all conditions though, the measurement location was maintained at 25 mm downstream from the injector nozzle with the adjustments being made on the horizontal plane (*i.e.* on the spray's footprint). Droplet size measurements were taken over 200 injections for all conditions. The total number of samples collected for each injection event was of the order of 25 samples per millisecond for each of the measured injections, resulting in more than 7500 valid droplet size and velocity measurements over the duration of the injection event for each test condition. The effect of temperature dependence of the refractive index of the fuels was considered on the basis of previously published work in this area, *e.g.* [18, 19].

A series of tests was also conducted by Laser-diffraction using a Malven Spraytec droplet sizer with 300 mm lens over a 36 element (log spaced) detector array. The two droplet sizing techniques operate on different principles and take measurements of different properties of spray; the Laser Diffraction system measures the droplet size along a beam (spatially averaged) whilst the PDA system is a fixed point measurement (temporally resolved). As such, these measurements are not directly equivalent; different factors are affecting each measurement as has been discussed in detail in the literature, *e.g.* see [20]. This will be further addressed in the results section. The Malvern system was aligned to measure along a line 30 mm downstream from the nozzle exit, *i.e.* 5 mm downstream the PDA's probe volume vertical location. This was due to geometric restrictions by the optical arrangements and differences will also be further addressed in the results section.

For laser diffraction droplet sizing individual plumes were required to be isolated in order to achieve enough optical transparency through the spray for measurements to be taken. Plume isolation was achieved by using a spray separator downstream from the nozzle itself to maintain the same internal flow within the nozzle for all conditions. Previous images of the spray development under a range of conditions have shown that the closely spaced spray plumes (plume pairs 2, 3 and 4, 5 in **Fig. 1**) show the greatest convergence under spray collapse condition, leading to the convergence of these plumes into a single dense spray plume. As these plumes showed the greatest development variation, plume 3 was selected as the separated plume for which the droplet size was

to be measured and the separator plate was so designed as to allow only plume 3 to pass through the plate under all spray development formations, including spray collapse.

Prior to measuring fuel spray droplets in the chamber, a rig was set-up to validate the simultaneous spray measurement using both the Malvern Spraytec and the TSI PDA system. A paint atomiser was filled with water and held open to provide a continuous source of droplets. The PDA system was aligned to measure the droplets in the centre of the spray and the measured SMD was 29 μm. The Malvern measured SMD was 25 μm, *i.e.* lower by ~14%. Considering that the Malvern also accounted for the fine droplets in the "mist" surrounding the main core of the spray, the difference between the two systems was within the expected range; further testing verified this by using the PDA to measure droplet sizes on the periphery of the water atomizer.

RESULTS AND DISCUSSION

SPRAY FORMATION

General Characteristics

Figs. 4–5 present spray images at 777 μs ASOI for Ethanol and Butanol, respectively, for 20–120 °C injector body temperatures, at 1.0 and 0.5 bar gas pressure. At nominally ambient conditions (20 °C, 1.0 bar), the alcohols exhibited broadly similar macroscopic spray form; this also resembled the spray form of Gasoline and *iso*-Octane at the same condition. However, as the pressure was decreased, spray formation was different between the two alcohols, primarily due to their differences in boiling temperature. Specifically, at 120 °C injector body temperature at 0.5 bar gas pressure, the nominal spray form is still maintained by Butanol, but it has 'collapsed' for Ethanol due to fuel 'flash boiling'. For more direct comparison and understanding, **Fig. 6** presents the macroscopic spray forms at 777 μs ASOI for all the fuels tested under the range of injector body temperature and gas pressure conditions. For Ethanol, the observed spray development is similar to that of Gasoline in that 'spray collapse' is observed to be complete at 120 °C, 0.5 bar. However, closer inspection of the plumes produced by Ethanol shows a clearer, more defined spray boundary than those of Gasoline at equivalent conditions. In this respect, the sprays produced by Ethanol are more similar to those produced by *iso*-Octane at low injector temperatures. In contrast, the spray development behaviour of Butanol appears to be similar to *iso*-Octane over the range of experimental conditions. For Butanol, as for *iso*-Octane, full spray collapse is not observed at 120 °C, 0.5 bar, which may be expected from Butanol's high boiling temperature. However, the Butanol sprays appear less well atomised than the *iso*-Octane sprays at injector body temperatures up to 90 °C, which is likely to be related to the higher viscosity and surface tension of Butanol, which both resist 'break-up'. Despite this, the Butanol spray can be seen to be somewhat converged at 120 °C, 0.5 bar, showing that the boiling temperature threshold has been surpassed at the given gas pressure.

Spray Plume Penetration

At the baseline ambient conditions of 20 °C injector temperature, 1.0 bar gas pressure all tested fuels were measured to have a similar spray plume penetration length for all captured time intervals ASOI, as illustrated in **Fig. 7**. A decrease in gas pressure decreases the drag force on the liquid spray droplets and hence leads to an increase in measured plume penetration at any given time interval. This effect can be seen by comparing **Fig. 8** (0.5 bar gas pressure) to **Fig. 7** (1.0 bar gas pressure), which also shows the effect to be particularly evident after approximately 600 μs ASOI. After this time interval, the increase in penetration length is approximately 10% with a halving of the gas pressure from 1.0 bar to 0.5 bar, although at a constant injector body temperature

there is little difference in the effect of the reduction in gas pressure for the different fuels. Prior to this time interval, the high spray momentum masks any measurable effect of gas drag on the plumes.

Increasing the injector body temperature appears to have only a small effect on plume penetration for a given gas pressure in the absence of spray collapse. This is illustrated in the plume penetration lengths being slightly longer at a gas pressure of 1.0 bar at 90 °C (**Fig. 9**) than at 20 °C (**Fig. 7**). This is likely to be due to the increase in fuel temperature leading to a reduction in the liquid viscosity, decreasing the fuel flow drag inside the nozzle and hence increasing its outlet velocity. A parallel plausible explanation for this increase in measured plume length is an increase in vaporisation of the spray, which acts to 'cloud' the spray tip and hence increase the plume length measurement, as can be seen at the spray tips at the appropriate condition in **Fig. 6**.

For an injector body temperature of 90 °C and gas pressure of 0.5 bar, the global spray images in F**ig. 6** showed a spray form relatively similar to the nominal, atmospheric form for most fuels, with the exception of *n*-Pentane which is seen to be collapsed at this condition. This has been quantified in **Fig. 10** where similar plume tip penetrations are illustrated for all fuels with the exception of *n*-Pentane.

At an injector body temperature of 120 °C at 1.0 bar gas pressure, a further small increase in plume tip penetration may be observed in **Fig. 11** for the un-collapsed fuel sprays at this temperature. The *iso*-Octane spray shows the least increase in penetration with increasing fuel temperature as its boiling point has not been sufficiently exceeded to promote measurable vaporisation of the spray. The *n*-Pentane spray at an injector body temperature of 120 °C shows full collapse, even at the 1.0 bar gas pressure condition, as illustrated in the images of **Fig. 6**. This is reflected in the much reduced plume tip penetration relative to the other, un-collapsed, fuel sprays due to the high liquid fuel evaporation rate from the plume tip, decreasing the measured plume axial length between the injector nozzle and the plume tip.

At a higher injector temperature of 120 °C at 0.5 bar gas pressure the increased evaporation of the fuel can be seen to greatly affect the spray development in **Fig. 6**, where the sprays produced by Gasoline, *n*-Pentane both show full spray collapse. For this condition a measurable difference in plume penetration lengths was observed between the tested fuels, as illustrated in **Fig. 12**. For the fuels that are seen to collapse at this condition a similar penetration curve is observed. *iso*-Octane and Butanol (that have the highest single boiling points) show the least spray collapse and hence the highest penetration rate. At 120 °C, the penetration of *n*-Pentane was slightly higher than that of Ethanol, due to the extreme rate of evaporation of *n*-Pentane and hence its respective reduction in droplet diameter at this condition (as will be discussed later), reducing the droplet drag to such an extent where the rate of plume tip penetration probably exceeds the rate of liquid fuel evaporation from the plume tip to cause a measurable increase in plume tip penetration over the collapsed sprays.

In summary, overall, an increase in fuel temperature initially leads to an increased measured plume penetration for all fuels due to decreased flow drag/friction and possibly an increase in fuel atomisation at the plume tip. However, a further increase in fuel temperature leads to a reduction in measured plume length once a critical vaporisation rate is surpassed, and the vaporisation rate becomes high enough to visually 'remove' the leading edge from the plume tip. These conflicting observations for a consistent trend are the possible reason that opposing views have been presented in the literature to date. For example, testing a multi-hole injector (of undisclosed configuration) using Indolene (a standardised Gasoline fuel) at a fuel pressure of 110 bar and gas pressure of 2.5 bar, Zhao *et al* [21] measured plume tip penetrations at 1.0 ms ASOI along the injector axis and

reported a measurement of 52 mm at 20 ° injector temperature. Then they showed a decrease in penetration with an increase in fuel temperature to 50 °C and 90 °C. This suggests that despite the higher gas pressure, the rate of evaporation of the fuel at the plume tip at the elevated temperature was greater than the rate of plume tip penetration, relative to the lower temperature condition. At a lower gas pressure of 1.0 bar, Zhao *et al.* [21] measured an increase in penetration with temperature from 58 mm at 20 °C to 63 mm at 90 °C injector body temperature. This suggests that at the given gas pressure, the effect of evaporation in reducing droplet diameter and hence drag was greater than that of the vaporisation of the liquid, potentially due to the difference in evaporation characteristics between the low and high volatility components of Indolene.

Analysis of the sprays produced by Ethanol and Butanol in the current work in comparison to those produced by the hydrocarbon fuels shows a consistent similarity of penetration between Ethanol and Gasoline, then Butanol and *iso*-Octane. This is more evident from the graphs showing the spray plume penetrations at the highest injector body temperature (**Figs. 11–12**), which is also the condition where the greatest difference between high and low volatility fuels is observed. However, even at colder conditions there are consistent trends between those pairs of fuels as analysed further in the next section on the rates of spray penetration.

Spray Plume Velocity

Spray tip velocities were quantified from the plume penetration measurements using a 'central-differencing' approach for all fuels in **Figs. 13–15**. Specifically, for Gasoline at the nominally ambient conditions (20 °C injector body temperature, 1.0 bar gas pressure) in **Fig. 13** an initial acceleration is observed to 444 μs ASOI due to the pressure acceleration of the fuel out of the nozzle, followed by a retardation due to the effects of aerodynamic drag and fuel evaporation. Overall, the measurements show a similar initial plume tip velocity for all the fuels at this condition but there is a slightly lower initial velocity for Ethanol and Butanol. These oxygenated fuels have approximately 2 to 6 times the viscosity, respectively, of the other tested fuels and this reduction in their initial velocities may be due to increased in-nozzle friction. A delay in seeing the alcohol fuels emerging from the injector tip has also been observed in-cylinder by the current authors [22], hence this is a consistent effect. At the ambient condition, the Butanol and Ethanol sprays continue to accelerate and show an increased velocity over the other fuels at subsequent measurement intervals. The greater density of these oxygenated fuels over the hydcrocarbons means that their spray momentum is greater for a given droplet size, and hence the effect of aerodynamic drag on reducing the droplet velocity is less pronounced.

Fig. 14 shows the measured plume tip velocity at an injector body temperature of 120 °C and gas pressure of 1.0 bar, at which only the low boiling point *n*-Pentane fuel is seen to fully collapse from the spray images. A higher initial spray velocity is measured than at 20 °C for the same gas pressure, due to reduced viscosity with increased temperature, except for *n*-Pentane which shows rapid evaporation and hence shorter measurable liquid plume penetration. Specifically for Gasoline **in Fig. 16**, an increase in injector body temperature to 90 °C at 1.0 bar increases the initial velocity by a small amount, due to a reduction in liquid viscosity in the nozzle hole. The global spray images do not show the spray to be collapsed at this condition. A reduction in pressure at 90 °C injector body temperature to 0.5 bar shows an increase in measured velocity at all time intervals ASOI due to a reduction in pressure having reduced the drag force. A further increase in injector body temperature to 120 °C at 1.0 bar gas pressure in **Fig. 16** shows a similar high rate of initial penetration as for the 90 °C, 0.5 bar condition as the rate of evaporation in reducing the droplet size and hence drag is again evident. However, a

rapid decrease in plume tip velocity is observed due to the evaporation of the fuel from the plume tip, shortening the measured penetration for these time intervals ASOI.

At the nominal spray collapse condition of Gasoline at 120 °C injector body temperature, 0.5 bar gas pressure, an increased initial velocity is measured over the ambient condition, due to the reduction in gas pressure, increasing the accelerative force on the spray through the nozzle as well as reducing the aerodynamic drag (**Fig. 15**). A high initial velocity is followed by a rapid reduction in acceleration due to the effect of liquid fuel evaporation. The un-collapsed fuel sprays in **Fig. 14** show a similar pattern to the un-collapsed sprays of **Fig. 15** but with reduced plume velocity due to the higher gas pressure. More specifically, The lack of spray collapse for *iso*-Octane is manifested by a further increase in spray tip velocity at 120 °C injector body temperature at 0.5 bar gas pressure over the lower temperature conditions (**Fig. 17**), although a greater rate of decrease in velocity is observed for this condition relative to the other conditions at later time intervals ASOI as the liquid has had sufficient time post injection for the rate of evaporation to cause a measurable reduction in the penetration rate of the spray tip. The similarity of velocities between Ethanol, Gasoline, Butanol and *iso*-Octane is again evident at this condition. The *iso*-Octane and Butanol sprays which both do not show collapse at this condition, exhibit an increased measured spray tip velocity over the collapsed fuel sprays, demonstrating the effect of evaporation for those fuels in reducing the plume length and hence measured spray tip velocity. At conditions of 120 °C, 1.0 bar in **Fig. 14**, the spray tip velocity of the Butanol spray again matches that of *iso*-Octane. The initial rate of penetration of Ethanol is slightly slower than that of Gasoline and, as also observed at lower fuel temperatures at 1.0 bar, the Ethanol spray appears to maintain its velocity for longer than the other fuels. The rate of evaporation of the liquid fuel is a key factor in determining the spray penetration velocity. Spray collapse conditions are associated with greater rates of evaporation and hence greater rates of decrease in plume tip velocity.

Spray Cone Angle

The angle of the outer envelope of the spray can act as a quantitative measure of the convergence of the plume for direct comparison between fuels. This external spray cone angle also has an important relevance to engine operation in that it indicates the position and area of the spray wetted footprint, and hence potentially un-burned hydrocarbons emissions from contact with the cylinder boundaries. However, the relationship between the overall spray cone angle and the wetted footprint is not straight forward. As the spray contracts, the cone angle decreases, which results in a smaller spray footprint. However, whilst the plume centre lines may contract, an increased ‘swelling’ of the plumes could also result in a larger measured cone angle. Whilst each individual plume may be seen to expand at the injector nozzle for spray-collapse conditions, the overall angle subtended by the extreme left and right-hand plume pairs, as imaged from the side, may actually be seen to decrease. This overall spray cone angle is of greater significance than the individual plume cone angles in relation to engine operation as it marks the outer boundary of the liquid spray and hence the rich air/fuel ratio area in the combustion chamber.

Furthermore, although an often used measure of spray convergence, there is no set definition of the measurement locations used to determine the spray cone angle. Furthermore, the ‘parabolic’ expansion nature of the spray’s shape near the nozzle, can lead to marked differences in measured angle values, even of the same spray, for different measurement locations. Zhao *et al.* [21] investigated the effect of measurement location on

measured cone angle for a typical pressure swirl spray, and ultimately concluded that the most appropriate location was purely dependent on the spray form and each investigator's preferences and requirements. In this respect, great care should be taken when comparing cone angle values from different sources. For multi-hole injectors, another important consideration when comparing overall spray cone angles is the nozzle hole diameter for individual plumes as well as the hole spacing and location on the injector tip. To this end, comparison may be made of the cone angles for individual plumes, although these are often impossible to measure for nozzles which produce more than one, closely spaced plumes, as was found to be the case for the injector used for this work.

For the purposes of the current work, two locations downstream from the nozzle were elected to define the spray's overall cone angle for a comparison between fuels. A near nozzle initial measurement location was first identified at 2 mm vertically downstream from the nozzle tip in order to avoid very near-nozzle spray development effects; then a second downstream location was identified 10 mm vertically from the upper measurement location. The cone angle formed by those two locations was found to be constant over the duration of the fully developed spray development for each experimental condition, and the results presented here are those measured from the images captured at 777 μs ASOI for all conditions (**Fig. 18**). At 20 °C injector body temperature and 1.0 bar gas pressure all fuels show a similar cone angle. The small differences in cone angles between the fuels at this condition are likely to be due to the evaporation of the liquid fuel from the plume boundaries, where *iso*-Octane evaporates less than Gasoline to bring about a slightly smaller measured cone angle. Conversely, the high rate of peripheral spray evaporation (to where it is no longer detectable by the imaging technique) of *n*-Pentane also acts to produce a narrower cone angle than the Gasoline.

This graph again illustrates the similarities in spray convergence behaviour between Ethanol and Gasoline, in that both sprays show a clear reduction in cone angle with an increase fuel temperature. However, the inclusion of lower boiling temperature, high volatility components in Gasoline is shown by a greater decrease in cone angle than for the single component Ethanol. By contrast, Butanol shows only a small increase in cone angle at 90 °C injector body temperature (similar to that seen for *iso*-Octane at 20 °C injector body temperature and 0.5 bar gas pressure) and at higher temperatures/lower pressures no reduction below its nominal angle at 20 °C, 1.0 bar. The fact that Butanol has a higher boiling temperature than *iso*-Octane again highlights the effect that the vaporisation rate has on causing spray convergence.

Spray Development Relationship to Fuel Properties

The difference between the fuel temperature and the boiling temperature of the fuel at the given gas pressure is known as the 'superheat'. For multi-component fuels, a range of superheat will be present in the fuel, although the driver for initial vaporisation will be the degree of superheat of the lowest volatility components. This appears to affect the rapidity of the vaporisation of the fuel, as evidenced in the difference in global spray forms at the high fuel temperature, low gas pressure condition in the previous paragraphs. The relative tendency for the tested fuels to collapse at 120 °C injector body temperature and 0.5 bar gas pressure may be directly compared to the fuel vapour pressures and bubble points shown in **Fig. 3**. The bubble point is the absolute ambient pressure at which a liquid will boil at the stated temperature, where increasing ambient pressure suppresses boiling and the formation of bubbles by exerting a greater force on the liquid surface. At a temperature of 120 °C, comparison of the fuel bubble points shows that the highest boiling pressure is for *n*-

Pentane, indicating that it is 'the most willing to boil' of all the fuels (*i.e.* the greatest ambient pressure is required to prevent the formation of bubbles), which is illustrated by the extent of its collapse at elevated fuel temperatures. In reference to the fuel's bubble points of **Fig. 3**, it may be observed that the spray collapses when the chamber gas pressure is at or below $1/10^{th}$ of the fuel's bubble point pressure at the given fuel temperature. For example, Gasoline is observed to collapse at 120 °C at 0.5 bar chamber gas pressure, which is approximately $1/10^{th}$ of its bubble point pressure at this temperature of 4.5 bar. Within the resolution of the temperature and gas pressure settings tested in this work, this trend appears to hold for all presented fuels, including those close to the transition values, such as at 90 °C injector body temperature and 0.5 gas pressure for Gasoline.

The trend of spray collapse for all fuels in relation to their vapour pressures and bubble points was followed further by increasing the injector body temperature to 180 °C and decreasing the gas pressure to 0.3 bar. This extreme condition was included to investigate whether the likely drivers of spray convergence held at higher temperatures, and whether 'instantaneous' flash-boiling of fuels would occur when an extent of superheat threshold was surpassed at that condition. **Fig. 19** shows that the spray produced by *iso*-Octane, which was not fully collapsed at 120 °C, was observed to fully collapse, indicating that the critical collapse threshold had been exceeded. At these test conditions the chamber gas pressure was below $1/10^{th}$ that of *iso*-Octane's vapour pressure, showing the continuation of this trend for these fuels. Butanol also followed the same trend.

The relationship between spray formation and bubble points is not widely discussed in the literature. In the one identified correlation which seeks to validate the computational modelling of pressure swirl sprays, van der Wege and Hochgreb [23, 24] note that bubble point calculations suggest that superheat of 20 °C is sufficient to bring about flash boiling which is rigorous enough to alter the spray form for pressure swirl sprays. For these, spray collapse is thought to be brought about by vaporised fuel being drawn to the low pressure core of the spray between the closely spaced plumes when the momentum of the fuel vapour being drawn to the spray core is sufficiently large to overcome the relatively low radial momentum of the fuel droplets for the plume form examined, causing these plumes to deviate and draw them together to form the collapsed spray observed. As such, the mechanism for spray collapse in pressure swirl sprays is likely to be different from that of multi-hole sprays, and hence pressure-swirl spray development appears more sensitive to the degree of fuel superheat than multi-hole spray development. Work by Wigley *et al*. [25] with pressure-swirl atomizers also noted that lower chain single component hydrocarbons, and in particular *n*-Heptane, appeared to be better than *iso*-Octane in simulating the volatility characteristics of Gasoline.

The spray characteristics of injectors also depend on the levels of turbulence generated by the internal flow upstream of the nozzle's exit. The effect of turbulence can be characterised by a Reynolds number, $Re = \rho u d/\mu$, where ρ and μ are the density and dynamic viscosity of the liquid fuel respectively, d is the nozzle hole diameter and u the flow velocity in the nozzle. The flow rate of the injector used in the current work was measured while injecting at a constant working pressure of 150 bar. This was divided by the number of nozzle holes so as to obtain the flow rate per nozzle hole. The jet velocity was obtained by dividing the nozzle mass flow rate by the product of the fuel density and the nozzle hole cross sectional area (the internal diameter of 0.2 mm was employed for this exercise); the velocity calculated was ~110 m/s, in agreement with the spray-tip velocity values obtained from the spray images when considering spray break-up and related momentum

effects. **Fig. 20** shows the *Re* plot for all the single-component fuels that were tested; the fluid properties of density and viscosity were obtained for varying temperatures along the liquid saturation curve. In the range 20–90 °C (293–353 K), the calculated *Re* numbers were 4,000–160,000, with Butanol's *Re* at 20 °C the lowest. Considering that *Re* is proportional to *Ud* and *U* is inversely proportional to d^2, if the nozzle's external diameter of 0.5 mm had been used instead of the internal 0.2 mm one, *Re* would have been 2.5 times lower for each fuel at each temperature, indicating conditions of laminar flow for Butanol at cold fuel conditions.

Figs. 21–22 present the calculated *We*ber, $We=\rho u^2 d/\sigma$, and the Ohnesorge, $Oh=We^{0.5}/Re$, numbers, respectively, for the single components selected and for the experimental temperature range of 20–120 °C (293–393 K), using a velocity of 110 m/s and as length scale the nozzle's inner diameter 0.2 mm. The *Oh* number shows gradual convergence to a single value of $\sim 5\times10^{-3}$ for all fuels at hot conditions, representing the similarity in all sprays at this collapsed condition in comparison to the *We* number that shows a clear separation between all fuels even at the extremes of injector temperature. The Ohnesorge diagram [26] is shown in **Fig. 23** with the Reitz and Bracco [27] defined break-up regimes superimposed. It is interesting to note that *n*-Pentane is well in the atomisation regime throughout the range of temperatures calculated, 7–120 °C (280–393 K). The heavy component of Gasoline *o*-Xylene is also in the atomisation regime and it only approaches the second wind induced regime at the coldest condition of 7 °C (280 K). Ethanol is in the atomisation regime too and it is only approaching the second wind induced regime at the coldest condition of 7 °C (280 K), similarly to *o*-Xylene. Butanol lies in the atomisation regime for temperatures higher than ~60 °C (333 K), similarly to Ethanol for temperatures higher than 20 °C (393 K), but it crosses over into the second wind induced regime at about 7–10 °C. This behaviour clearly demonstrates the implications for engine cold-start conditions.

NEAR NOZZLE IMAGING

To better observe the break-up mechanisms leading to the different envelopes of spray formations (*i.e.* spray plume convergence and collapse), spray break-up was investigated by high magnification imaging of the spray in the near nozzle regions. As mentioned earlier, the injector nozzle used for this work is of a stepped design, with the smaller diameter orifice, which forms the fuel flow path, being recessed from the nozzle's outer surface. This small orifice (0.2 mm) opens up to a larger diameter orifice (0.5 mm), which is that seen at the nozzle surface. As such, the fuel imaged at the injector tip is actually ~0.5 mm downstream from its actual injection location at the end of the small orifice, hence the plumes may have started to break-up already due to effects upstream of where they can first be imaged.

Backlit shadowgraph images of the spray were captured to illustrate the 'first fuel site' during initial spray development, the steady-state injection process, as well as the spray form in the near-nozzle region at the end of injection. The plume tip penetration at initial spray development was measured to be ~1.0 mm per frame interval (20 μs), equivalent to a tip velocity of ~50 m/s, *i.e.* in line with the spray tip velocities measured from the global spray images. The spray shape for the 'very first' fuel as seen at the injector tip appears to be very similar for all test conditions. This is broadly the case also for those conditions at which spray convergence and collapse are observed in the global spray form. Specifically, each plume pair is clearly defined with a gap evident between each plume, including the closely spaced plume quartet on the right hand side of the image. For the high temperature conditions, the sprays are wider at the nozzle exit than for the ambient conditions,

suggesting some widening and expansion of the spray plume between its injection location and the nozzle surface. However, combination of the plumes is not yet evident at this stage for any of the test conditions.

The second frame, captured 20 μs later than the frame showing 'first' fuel, continues to show clearly defined plume pairs for the un-collapsed spray conditions of Gasoline (top row of **Fig. 24**). However, at the same time interval after the start of injection at an injector body temperature of 120 °C and a gas pressure of 0.5 bar, the closely spaced plumes on the right hand of the image have combined and individual spray plumes are now more difficult to discern (middle row of **Fig. 24**). This indicates the start of spray collapse during the transient injection process. As may be expected, the global spray form is reflected in the steady state sprays in the near nozzle region. In a similar reflection of the global spray form at this time interval, the *iso*-Octane spray shows some coming together but less widening of the plumes at the injector tip than is evident for Gasoline and individual plume tips can still be easily made out with a clear gap between the plume tips (**Fig. 25**).

Interestingly, the greatest spray plume width increase is seen at the higher gas pressure condition images at the highest injector body temperatures (1.0 bar), even though this condition does not lead to the same level of spray convergence as the low gas pressure condition. For some collapse conditions, individual plume tips can still be made out, although the trajectory of convergence of the plumes is highly evident (e.g. *n*-Pentane at 90 °C injector body temperature, 0.5 bar gas pressure in **Fig. 26**).

At pintle closing (row four) the throttling action of the pintle at the nozzle orifice inlet reduces the extent of plume interaction and hence plume separation is once more evident for all conditions. This reduction in fuel flow and hence spray velocity and break-up energy can be seen to lead to the formation of large droplets. The size and low break-up rate of these droplets may be expected to adversely affect vaporisation and mixing, and hence affect engine out un-burned hydrocarbon emissions.

Images of the left-hand-side plume of **Figs 24–26** (*i.e.* plume 1) were also captured with Laser sheet pulsed illumination at emergence from the injector nozzle to capture the initial spray, then at 800 μs ASOI to capture the steady state injection process and finally at 2000 μs ASOI to capture the end of injection with Gasoline and *iso*-Octane as shown in **Figs. 27**. These allowed clearer visibility of the spray's leading edge locally and cone 'surface' in comparison to the backlit technique. The initial Gasoline spray at the nominally ambient conditions (20 °C injector body temperature, 1.0 bar gas pressure) shows clearly discernable individual liquid ligaments and droplets at and around the leading edge of the spray. These features were also evident in the initial spray images at the nominally ambient conditions for the *iso*-Octane sprays. The steady state spray plume has a well defined boundary and again individual features on the boundary and plume surface can be depicted. Likewise, the end of injection image shows a number of larger droplets associated with the reduced break-up energy in the spray as the pintle closes at the end of the injection event. The clarity of these features suggests that they are in a steady state in relation to the image integration time of 20 μs, and hence that the effect of evaporation or other mechanism to bring about a flux in the spray over this time interval is small under these conditions.

At 120 °C injector body temperature, 0.5 bar gas pressure, the increased level of evaporation was evident. For Gasoline in **Fig. 27**, the spray boundaries and leading edge are no longer clearly defined and there is a gradual reduction in pixel brightness between the white liquid spray and the surrounding black background. The imaged plume bulges as it exits the nozzle and the darker shading to the right of the plume suggests a 'solid' cylindrical form to the initial plume. In both the Initial Spray and Steady State Spray images the adjacent plume can be

seen in this image due to the increased girth of the plumes. At the End of Injection some large droplets are evident 'suspended' in a hazy mist likely to be due to the small droplets which are present at the spray periphery, formed due to the evaporation of the spray as it exits the nozzle. These general observations also relate to the near nozzle spray produced by *iso*-Octane, although the higher boiling temperature range of these fuels is reflected in their near nozzle spray behaviours. The spray produced by *iso*-Octane shows a number of larger droplets within and around the spray, relating to a greater resistance to break-up than Gasoline.

It is clear that even using very high-speed imaging of the initial emerging spray, spontaneous and complete evaporation was not observed for any gas pressure and temperature conditions. Specifically, a finite time is required for the rate of evaporation to increase to sufficient levels to cause the plume tip to expand. The fact that the fully developed spray characteristics are not displayed at the injector until 20 μs after the 'first fuel' seen at the injector tip would appear to indicate that even at the most extreme vaporisation rates a timescale of the order of 20 μs is one of the determining factors in the development of equilibrium conditions between the liquid fuel and surrounding gas, leading to the existence of an external spray break-up length.

The imbalance between the fuel's internal thermal energy and that of the gaseous body is the extent of superheat present within the fuel. Within the confines of the injector flow path, the liquid pressure allows large degrees of superheat to be contained in the fuel. Therefore, as 'flash boiling' starts to occur the evaporation process takes heat away from the liquid and cools it down, which in turn inhibits 'flash boiling' and brings about a form of equilibrium. Hence, it may be said that the level of superheat is important in two ways for the spray. Firstly it can influence the time taken for the spray to begin to rapidly vaporise, since it is a measure of the 'thermodynamic driving force' for moving the system towards equilibrium, and secondly that it influences the amount of vapour that is produced during the boiling process. For multi-component fuels, a range of superheat will be present in the fuel, although the driver for initial vaporisation appears to be the degree of superheat of the lowest volatility component and it may be re-iterated that the degree of superheat was sufficient to lead to spray collapse when the chamber gas pressure was at or below 10% of the fuel's bubble point or vapour pressure at the given fuel temperature.

DROPLET SIZING

Phase Doppler Droplet Sizing

The character of the injection event in terms of the droplets detected and measured is shown in **Fig. 28**; the diagram refers to Gasoline at 20 °C, 1.0 bar. A high number of droplets are detected in the initial spray as it passes the detection area. However, due to the high liquid density during the course of the main part of the injection event, the detection rate reduces during the spray event. Towards the end of injection the number of detected droplets increases again as the closing of the injector pintle reduces the liquid volume flow rate (2000–3000 μs ASOI). Lastly, a number of droplets entrained in the plume wake are detected following the injection event.

The mean droplet sizes during the injection event have been collated in **Figs. 29–31** for Gasoline, *iso*-Octane and *n*-Pentane, respectively. These represent averaged values over 100 μs intervals for all 200 injection events per fuel and condition. For nominally ambient conditions (20 °C, 1.0 bar), a similar trend in drop size over the spray duration may be seen for all fuels. Relatively large droplets are measured at the spray tip (leading edge), with an ensuing reduction in mean droplet size during the remainder of the spray. More specifically, the initial

mean droplet diameter for Gasoline at 20 °C, 1.0 bar, is around 15 µm, and is seen to diminish over the main injection's duration to values around 11–12 µm; however, droplet sizes as large as 30 µm and as small as 2 µm were measured (as shown earlier in **Fig. 28**). The initial and mid-injection droplet size mean values for *iso*-Octane in **Fig. 30** are similar to those measured for Gasoline in **Fig. 29**. The droplets at the leading edge of the *n*-Pentane spray though are slightly smaller than for Gasoline and *iso*-Octane (~14 µm), indicating a more rapid initial break-up for the *n*-Pentane spray. The mid-injection mean droplet size is also slightly lower for *n*-Pentane in **Fig. 31** than for the other fuels (~10 µm), potentially a result of *n*-Pentane's higher volatility and lower viscosity relative to *iso*-Octane and the majority of components in Gasoline.

Increasing the injector body temperature to 120 °C at 1.0 bar, results in fewer large droplets being detected at the start of the injection event, with the initial mean reduced to around 10 µm and the mid-injection mean being centred at around 9.5 µm for Gasoline. The global spray images at this condition (**Fig. 6**) show some convergence of the spray plumes but not a complete collapse of the spray form. For *iso*-Octane, an increase in the injector body temperature to 120 °C at 1.0 bar gas pressure shows a reduction in the initial mean droplet size, although this decrease in initial droplet size is not as great as for Gasoline. Post-injection droplets are of a more constant, and smaller, size than those measured at the ambient condition of 20 °C, 1.0 bar for *iso*-Octane (**Fig. 30**) and are similar in size to those measured with Gasoline at this condition (**Fig. 29**). For *n*-Pentane, an increase in injector body temperature to 120 °C leads to spray collapse for this high volatility fuel and this is reflected in a reduction in both the initial and mid-injection mean droplet sizes to 8 µm (**Fig. 31**).

Decreasing the gas pressure from 1.0 bar to 0.5 bar for an injector body temperature of 120 °C leads to relatively more stable mean droplet size over the entire spray duration, including its leading edge, for *iso*-Octane. For Gasoline and *n*-Pentane, the mean droplet diameter is lower than that for the nominally ambient conditions of 20 °C, 1.0 bar, though is highest for *iso*-Octane indicating the lowest rate of spray break-up and evaporation for the un-collapsed *iso*-Octane spray pattern at this condition. For Gasoline, the reduction in gas pressure from 1.0 bar to 0.5 bar at 120 °C resulted in a small decrease in initial mean droplet size from 12 to 10 µm. This reduction in pressure for Gasoline induces spray collapse and results in a further reduction in measured droplet diameter over the course of the injection event as illustrated in **Fig. 29**. At this collapse condition the initial mean droplet diameter is around 9 µm and the mid injection mean is around 7 µm.

The spray produced by *n*-Pentane, which was the most collapsed at 120 °C, 0.5 bar (**Fig. 31**) has the lowest mean droplet size of the tested fuels. The similarity in small droplet size at the leading edge of the Gasoline spray to that of *n*-Pentane may be an indication of the initial rapid break-up of the Gasoline spray, driven by its high volatility components and resulting in spray collapse under these conditions. The decrease in gas pressure from 1.0 bar to 0.5 bar at 120 °C leads to a small further reduction in initial and mid-injection mean droplet size to around 7 µm. For both those spray-collapsed conditions with *n*-Pentane, high data rates were captured during the mid-injection period (and no post spray droplets), indicating lower spray densities compared to the other fuels and higher vaporisation rate of *n*-Pentane.

The trends in droplets size shown in **Figs. 29–31** show a consistency between the mean droplet diameter and break-up rate in relation to the global spray development images. For all measurements the trend is for a reduction in droplet size with increasing injector body temperature. A similar trend was observed in relation to the gas pressure, where the graphs show that a reduction in gas pressure leads to a reduction in measure droplet

size for a given injector body temperature. The next section compares the trends observed from the Phase Doppler and Laser Diffraction techniques in terms of Sauter Mean Diameter (SMD).

Sauter Mean Diameter – Comparisons and Analysis

The SMD diameter measured by both the Laser Diffraction and Phase Doppler techniques are presented **Figs. 32–34** for Gasoline, *iso*-Octane and *n*-Pentane respectively. It needs to be reiterated here that the PDA results were acquired at a point source 25 mm along the *z*-axis below the injector nozzle in the centre of Plume 2 whilst those for the Laser diffraction measurements in these graphs are across the diameter of Plume 3, 30 mm along the *z*-axis below the injector tip. However, due to the similarity in these plumes' reactions to the experimental conditions, and the measurement location, qualitative comparisons of the trends obtained by these techniques at these locations are deemed to be valid if potential sources of variation between the measurements obtained with the different techniques are considered.

The measurements obtained with the two techniques differ consistently by approximately 50%. Although a nominal difference of 14% in droplet sizes was measured between the systems during calibration, the larger difference in actual measurements may be attributed to a number of factors. A small portion of the difference is due to the difference in distance from the injector tip at which the different techniques were applied. The average droplet size tends to reduce downstream from the injector nozzle due to various modes of droplet collision and simultaneous droplet evaporation. Therefore, a small reduction in droplet sizes acquired at the further downstream Laser Diffraction location of measurement in comparison to Phase Doppler's probe-volume location may be attributed to this and tests showed that such a contribution to the differences obtained was ~5–10%. The different plumes in which the measurements were taken may also have contributed to the difference in measured droplet sizes. More specifically, the fuel flow through the nozzle's interior geometry can lead to effects on the degree of atomisation of the fuel, as observed in optical nozzle work [9, 10]. To this end, the difference in interior turning angles of the nozzle holes for plume 2 and Plume 3 is likely to have played a role in the difference in measured droplet sizes, *albeit* not quantified in detail yet. However, the main consideration should be to the difference in the nature of the techniques used; the PDA is a point measurement technique whereas the Laser Diffraction system acts along a line of sight through the spray plume. Therefore, the latter captures a higher number of smaller droplets along the beam, reducing the average measured droplet diameter. Nevertheless, even after consideration of these sources of difference, the droplet size trends measured with the different techniques in relation to the matrix of experimental conditions employed are highly consistent and a number of observations can be made in relation to how spray development is affected by the break-up rate.

For Gasoline and *n*-Pentane, increasing the injector body/fuel temperature can be seen to steadily decrease the measured SMD. For Gasoline **Fig. 32** this reduction becomes more pronounced closer to the nozzle which shows a sharp reduction in droplet size as the spray collapse condition is approached. The droplet sizes measured for *iso*-Octane show little variation with increasing temperature until the highest test temperature of 120 °C is approached (**Fig. 33**). This is reflected in the spray images which show little variation except some slight convergence at this highest test temperature, low pressure condition. This rapid reduction in measured droplet size suggests that the rate of break-up and/or vaporisation increases once the boiling point of the fuel (98 °C for *iso*-Octane at 1.0 bar) has been exceeded. This would also be valid for *n*-Pentane (**Fig. 34**), where its

boiling temperature of 36 °C at 1.0 bar is exceeded between the lowest two test temperatures, and hence a sharp reduction is not observed due to the lack of resolution in the elected temperature step changes.

There are no other main data in the literature on fuel atomisation from multi-hole DISI injectors at high temperature 'flash-boiling' conditions in order to compare the current data with. However, a similar trend between droplet size and onset of collapse has been observed with pressure-swirl atomisers. Specifically, using a "multi-component petroleum product" at a fuel temperature of 90 °C van der Wege and Hochgreb [23, 24] measured an SMD of approximately 16–19 μm at 25 mm from the injector tip at the spray-collapse condition for that injector. It should be borne in mind though that pressure swirl sprays collapse under an increase in gas pressure too, apart from an increase in fuel temperature. van der Wege and Hochgreb [23, 24] noted that the exact value of the SMD was a function of the radial distance from the injector axis. Although these droplets are slightly larger than those measured for the multi-hole injector investigated for this work, the increased fuel pressure and the alternative form of atomisation utilised would both lend themselves to the production of smaller droplets. The spray collapse condition was found to occur at a gas pressure of 0.6 bar and an injection pressure of 50 bar in [23, 24]. Nonetheless, the similarity of relevant conditions and measured droplet sizes both suggest similar spray break up rates leading to spray collapse.

For the current work, initial convergence of the far right plume pair appears to occur when the measured SMD falls below ~12 μm from the images in **Fig. 32** overlaid on the measured droplet sizes for Gasoline. This suggests that there is a critical droplet size at which deviation from the nominal spray form can occur. In combination with the spray images previously presented, an increase in fuel temperature and/or decrease in gas pressure has been shown to lead to a gradual increase in break-up and droplet vaporisation rate. These operational parameters act in relation to the fuel properties to reduce the size of the droplets produced at any given location downstream of the injector nozzle. The droplet sizing work appears to show that once the droplets are below a certain critical diameter, possibly in relation to the liquid density, their momentum along the spray plume trajectory is diminished to the extent that they are drawn into the low pressure region in the centre of the spray, and their migration to this region acts to draw the plumes together. At another critical break-up rate value, both the rate of migration and the number of migrating droplets combined, act to converge the spray plumes into the 'collapsed' formation. The droplet results and the 'extreme condition' imaging results at 180 °C also suggest that any further increase in the break-up rate acts to accelerate the plumes along their collapsed central axis and increase the vaporisation rate further. It is interesting that similar trends have been observed by the current authors using a slightly different multi-hole injector with E85 (85% Ethanol, 15% Gasoline blend), hence the study was not repeated with Ethanol within the bounds of the current work.

Despite being a fundamental consideration in the modelling of sprays, the difficulty in relating a representative droplet dimension to the prevailing conditions has prevented any such relationships being established for Gasoline sprays at typical direct injection pressures. As with other aspects of Gasoline direct injection, the most applicable research is that relating to Diesel sprays. Hiroyasu *et al.* [28, 29] attempted to develop a quantitative relationship for the droplet size in terms of the SMD, based on Laser Diffraction droplet size measurements for a diesel spray injected at 900 bar into a gaseous atmosphere at 30 bar, and derived the following relationship (where d is the nozzle diameter and all other nomenclature has its usual meaning.):

$$SMD = 0.38dRe^{0.25}We_L^{-0.32}\left(\frac{\mu_L}{\mu_G}\right)^{0.37}\left(\frac{\rho_L}{\rho_G}\right)^{-0.47} \quad \textbf{(1)}$$

Applying this relationship to the conditions of the current work yielded the droplet sizes in **Fig. 35**. It is quite interesting that, despite its Diesel origin, **(1)** represents reasonably well the trends in droplet size reduction with increasing temperature and decreasing gas pressure for all fuels; it also predicts SMD with ~50% difference from the Laser Diffraction measurements of **Figs. 32– 34**. Therefore, it seems plausible that this relationship could be used to predict the average SMD for typical DISI engine sprays if the values of constants were further refined. However, it would probably be also desirable to include the cavitation number in **(1)**, as in-nozzle phase-change phenomena have been explicitly observed in multi-hole injectors of the same type [9, 10].

Droplet Velocities

The behaviour of droplet velocities is presented in **Fig. 36** for *iso*-Octane. These values have been calculated from the square root of the sum of the squares of the *y* and *z* axis velocity components measured simultaneously by PDA. Due to the side view imaging of the spray from which the previously presented spray tip velocities were calculated (same *y*-*z* view), both these velocity measurements are comparable. The analysis is focused on *iso*-Octane that maintained its spray directionality at all conditions, hence direct comparison with the imaging data is meaningful. However, the reader needs to remember that the Phase Doppler technique is spatially bound, *i.e.* it measures any droplet which happens to pass through the fixed measurement location, whilst the previously presented data for *iso*-Octane in **Figs. 17** are spatially dynamic, *i.e.* they refer to the velocity of the spray's leading edge at all times, regardless of the spatial location of the edge.

The droplet velocities just past the spray's leading edge earlier than 600 μs ASOI (*i.e.* the first droplets which could be measured), were in a narrow band of 40–60 m/s with an average of ~50 m/s. The steady-state spray measured from approximately 700 μs ASOI onwards is formed of droplets with a band of velocities in the range 10–90 m/s, with a slightly increased average value over those droplets measured prior to this period. The mean velocity is then seen to tail off with a reduction in value, although some higher velocity droplets appear to have been captured later in the spray (1200 μs ASOI).

The *iso*-Octane spray droplet velocities at 20 °C and 0.5 bar show a more distinctive increase following the leading edge than at 1.0 bar, but with the same trailing off in mean velocity. Overall, the mean velocity is higher at 0.5 bar than at 1.0 bar due to reduced drag on the droplets; droplets as fast as 120 m/s were captured within 500–700 μs ASOI. An increase in injector body temperature to 120 °C is seen to increase droplet velocities at a gas pressure of 1.0 bar relative to 20 °C. The range of velocities of droplets following the initial spray also increases, with individual droplets having measured velocities over 120 m/s and the mean velocity being around 60 m/s throughout the spray duration. Although *iso*-Octane does not collapse at this condition, it is above or at its boiling temperature of 99 °C at 1.0 bar whilst in residence in the injector, therefore, upon opening of the injector orifice, in-nozzle 'flash boiling' can accelerate the initial volume out of the injector, resulting in the high measure droplet velocities occurring early on in the spray. The effect is more accentuated at 120 °C, 0.5 bar, with similar mean initial velocity values as at 1.0 bar but with a wider range of droplet velocities exceeding 130–140 m/s throughout the initial and steady state phase of the spray. The increase in mean velocity is then clearer and steadier up to ~1200 μs ASOI in comparison to 1.0 bar.

In order to investigate the presence of a linkage between the measured droplets size and its velocity within the spray plume, the correlation coefficients between these parameters were calculated. The linkage was quite weak at the nominally ambient condition of 20 °C injector body temperature, 1.0 bar gas pressure with a correlation coefficient of just 0.14. Decreasing the gas pressure to 0.5 bar led to an almost identical correlation coefficient of 0.14, verifying the weak relationship between velocity and droplet size at 20 °C. Increasing the injector temperature to 120 °C at 1.0 bar made the correlation a bit stronger with a calculated correlation coefficient of 0.19. A reduction in gas pressure to 0.5 bar at that high temperature resulted in the strongest correlation of 0.24. Comparison of spray velocity values obtained from plume penetration imaging and droplet sizing shows that the image-based measurement essentially detects the fastest and largest droplets in the spray that form the dense leading edge of the spray. In fact, the spray tip velocity lines in **Fig. 17** roughly followed the 'horizon' of the largest velocities measured by the Phase Doppler technique.

Considering that the Weber number in **Fig. 21** was based on the diameter of the nozzle and the flow velocity in the nozzle (200 μm, 110 m/s, respectively), using a mean droplet size of about one order of magnitude smaller than the nozzle diameter (**Fig. 30**) and a velocity of about half that in the nozzle (**Fig. 36**), the representative Weber number for the droplets is about two order of magnitude lower than the values shown in **Fig. 21**.

SUMMARY AND CONCLUSIONS

The current paper studied the mechanism of atomization from a multi-hole injector with Gasoline, *iso*-Octane, *n*-Pentane, Ethanol and *n*-Butanol. A range of injector body temperatures and gas pressures were considered and both high-speed spray imaging and droplet sizing techniques were applied. A range of parameters were quantified, including spray penetration, cone angle, droplet sizes and velocities. The conclusions of this study are listed below in subsections in order to summarise as clearly as possible the observed effects:

General Observations

- At 20 °C, 1.0 bar, both alcohols exhibited broadly similar macroscopic spray forms that also resembled the sprays of Gasoline and *iso*-Octane. However, at 120 °C, 0.5 bar, the nominal spray form had 'collapsed' for Ethanol but it was maintained for Butanol.
- For Ethanol, the observed spray development was similar to that of Gasoline in that 'spray-collapse' was complete at 120 °C, 0.5 bar. However, closer inspection of Ethanol's plumes showed a better-defined boundary than Gasoline's; in that respect, Ethanol sprays were more akin to *iso*-Octane at low temperatures.
- The macroscopic spray 'envelope' of Butanol was similar to *iso*-Octane's over the range of test conditions. However, Butanol appeared less well atomised than *iso*-Octane up to 90 °C which was likely due to higher viscosity and surface tension effects. For both Butanol and *iso*-Octane full spray-collapse was not observed at 120 °C, 0.5, but Butanol plumes bar exhibited much better atomisation than at 90 °C.
- High magnification near-nozzle imaging showed that the spray shape for the 'first' fuel seen at the injector tip was broadly similar for all conditions. At un-collapsed spray conditions, images 20 μs later than 'first fuel' continued to show clearly defined plume pairs as expected but *iso*-Octane exhibited a number of larger droplets within and around the spray than Gasoline. At high temperature conditions the sprays were wider at the nozzle exit than at 20 °C but combination of plumes was not evident.
- 20 μs after 'first fuel' at 120 °C, 0.5 bar, Gasoline's plumes had already started to combine, indicating the beginning of spray collapse during the transient injection process. For other spray-collapse conditions,

individual plume tips could still be made out, although a trajectory of plume convergence was evident, *e.g.* *n*-Pentane at 90 °C, 0.5 bar. The fact that fully-developed collapsed spray characteristics were not displayed close to the nozzle exit until 20 μs after 'first fuel' indicated that even at the most extreme vaporisation rates a timescale of that order was a determining factor in the development towards 'equilibrium' between liquid fuel and surrounding gas. At the end of injection plume separation was again evident even at fully collapsed conditions as the throttling action of the pintle at the nozzle's inlet reduced the extent of plume interaction.

- The initial spray development of Gasoline and *iso*-Octane at 20 °C, 1.0 bar showed clearly discernable individual liquid ligaments and droplets at and around the leading edge of the spray. The end of injection also showed a number of larger droplets; the size and low break-up rate of these may affect adversely vaporisation and mixing, hence contribute to increased engine-out hydrocarbon emissions.

Spray Penetration

- At 1.0 bar, 20 °C, all fuels had similar spray plume penetrations during injection; when the gas pressure was halved to 0.5 bar there was an increase in penetration by ~10% for most fuels. Increasing the injector temperature had a small effect on penetration for a given gas pressure in the absence of spray collapse; penetrations were typically ~10% longer at 90 °C, 1.0 bar. This was likely due to decreased in-nozzle flow friction and enhanced atomisation at the spray tip which 'swelled' the plumes. At 90 °C, 0.5 bar sprays had similar form to 20°C, 1.0 bar for most fuels, with the exception of *n*-Pentane which was fully collapsed.
- Similar initial plume tip velocities (earlier than 444 μs ASOI) were measured for all fuels at 20 °C, 1.0 bar, typically in the range 80–90 m/s, with slightly lower velocities for Ethanol and Butanol. However, both alcohols showed an increased velocity at subsequent measurement intervals. It is believed that the greater density of the alcohols over the hydcrocarbons' leads to greater momentum for a given droplet size and hence less pronounced effect of drag on droplet velocity.
- At 120 °C, 1.0 bar, a further small increase in penetration was observed for the un-collapsed sprays. *iso*-Octane showed the least penetration increase with increasing temperature. *n*-Pentane showed full collapse at 120 °C even at 1.0 bar. This was reflected in reduced penetration relative to the un-collapsed fuel sprays, attaining plume tip velocities of ~70 m/s in comparison to 90–100 m/s for the other fuels.
- At 120 °C, 0.5 bar, a large difference in plume penetration was observed between various fuels (~20%). For the collapsed sprays a similar penetration curve was observed, with *n*-Pentane exhibiting slightly higher penetration than Ethanol. This was attributed to the high rate of evaporation of *n*-Pentane and respective reduction in droplet sizes, decreasing drag to the extent that the rate of penetration probably exceeded the rate of evaporation from the plume tip. A similarity of velocities between Ethanol and Gasoline, as well as Butanol and *iso*-Octane, was evident. The un-collapsed *iso*-Octane and Butanol sprays exhibited higher velocity than the collapsed fuel sprays. For *iso*-Octane this was manifested by a further increase in spray tip velocity (~110 m/s) in comparison to lower temperatures, although a greater rate of decrease in velocity was observed at later intervals (the liquid had sufficient time post nozzle-exit for evaporation to cause a measurable reduction in penetration rate). Ethanol maintained its plume velocity for longer than the other fuels.

Spray Cone Angle

- At 20 °C, 1.0 bar, all fuels showed similar cone angles, typically 95°–100°. Any small differences were likely due to atomisation and evaporation from the plume boundaries, as *iso*-Octane atomised less than Gasoline and brought about a slightly smaller cone angle (*i.e.* less plume 'clouding' was captured). Conversely, the high rate of peripheral spray evaporation of *n*-Pentane produced a narrower cone angle than Gasoline.
- Both Ethanol and Gasoline sprays showed a clear reduction in cone angle with an increase in injector temperature. The effect of high volatility components in Gasoline was manifested by a greater decrease in cone angle than for Ethanol. In contrast, Butanol showed very small changes in cone angle. The lowest cone angles were measured for Gasoline and *n*-Pentane at 120 °C, 0.5 bar (~80° and ~70° respectively), whilst Ethanol's was about 85°. The changes in *iso*-Octane's cone angle were between Gasoline's and Ethanol's.

Fuel Properties and non-Dimensional Numbers

- In reference to vapour pressures and bubble points it was observed that the spray was collapsed when the gas pressure was at or below ~10% of the fuel's bubble point or vapour pressure at the given temperature. Temperatures as high as 180 °C and gas pressures as low as 0.3 bar were considered and, within the resolution of steps tested in this work, this trend appeared to hold for all fuels.
- The calculated *Re* numbers for all fuels were 4,000–160,000 over 7–180 °C with Butanol's *Re* the lowest, indicating conditions of laminar/turbulent transition at cold fuel conditions. The *Oh* number showed convergence to a value of $\sim 5 \times 10^{-3}$ for all fuels at collapsed spray conditions, representing well the similarity in spray behaviour in comparison to the *We* that showed distinct separation between fuels. Study of the Ohnesorge diagram showed that *n*-Pentane was always well in the atomisation regime throughout the range of 7–120 °C (280–393 K). The heavy component of Gasoline *o*-Xylene was also in the atomisation regime and it only approached the second wind induced regime at the coldest condition of 7 °C (280 K). Ethanol was in the atomisation regime too and it only approached the second wind induced regime similarly to *o*-Xylene. Butanol was in the atomisation regime for temperatures higher than ~60 °C (333 K), similarly to Ethanol for temperatures higher than 20 °C (393 K), but it crossed over into the second wind induced regime at about 7–10 °C.

Droplet Sizes and Velocities

- Phase Doppler measurements showed similar trends in droplet sizes during the injection event at 20 °C, 1.0 bar for all hydrocarbons. Relatively large droplets were measured at the spray's leading edge with an ensuing reduction in droplet sizes during the remainder of the spray. The initial ensemble-averaged droplet diameter for Gasoline at 20 °C, 1 bar was ~15 µm and was seen to reduce over the injection to ~11 µm; however, individual droplets as large as 30 µm and as small as 2 µm were caprured. The droplets at the leading edge of *n*-Pentane were slightly smaller than Gasoline's and *iso*-Octane's (~13 µm). The mid-injection average droplet size was also slightly lower for *n*-Pentane than for the other fuels (~10 µm), potentially a result of *n*-Pentane's higher volatility and lower viscosity.
- The SMD illustrated critical differences between Gasoline, *iso*-Octane and *n*-Pentane. At 20 °C, 1.0 bar, the SMD was ~15–17 µm for all fuels. For Gasoline and *n*-Pentane, increasing the injector body temperature steadily decreased the SMD. In contrast, *iso*-Octane's SMD showed only little variation with increasing

temperature until 120 °C was approached. The rapid reduction in SMD at 120 °C and beyond at 0.5 bar suggested that the rate of break-up and/or vaporisation had increased greatly once the boiling point of *iso*-Octane had been exceeded. This observation would also be valid for *n*-Pentane between the lowest two test temperatures of 20 °C and 50°C; however, such a sudden sharp reduction was not observed due to the lack of resolution in the temperature step changes and, hence, requires further study.

- Initial spray plume convergence appeared when the SMD fell below ~12 μm. This suggested that such a size led to diminished droplet momentum along the spray's plume trajectory to the extent that droplets were drawn into the central spray region and this migration acted to pull the plumes together into a 'collapsed' form. At higher temperatures than that at the onset of spray collapse, any further increase in break-up acted to accelerate the plumes along the spray's collapsed central axis and increased the evaporation rate further.
- Droplet velocities were analysed for *iso*-Octane; over the first 600 μs ASOI, these were in a narrow band of 40–60 m/s with an average of ~50 m/s. The steady-state spray from ~700 μs ASOI onwards was formed by droplets of 10–90 m/s with a slightly increased average than 50 m/s. Overall, the mean velocity was higher at 0.5 bar than at 1.0 bar due to reduced drag; droplets as fast as 120 m/s were captured within 500–700 μs ASOI. Raising the temperature to 120 °C at 1.0 bar increased the droplet velocities relative to 20 °C. The range of velocities following the initial spray also increased with individual droplets attaining over 120 m/s, whilst the mean was ~60 m/s over injection. The effect was accentuated at 120 °C, 0.5 bar, with similar mean initial values as at 1.0 bar but with larger number of droplets exceeding 130 m/s throughout injection.
- The largest velocities measured by PDA were as high as the spray plume tip velocities quantified by imaging. The linkage between droplet sizes and their velocities was quite weak, especially at 20 °C, 1.0 bar with a correlation coefficient of 0.14 at both 1.0 and 0.5 bar. Increasing the injector temperature to 120 °C at 1.0 bar made the correlation a bit stronger with a correlation coefficient of 0.19. A reduction in gas pressure to 0.5 bar at 120 °C resulted in the strongest correlation of 0.24.

Current work is focused on further spray imaging and droplet-sizing of the alcohols and other bio-components over a range of blending ratios with Gasoline. Development of faithful empirical models for SMD as a function of fuel properties is also of strong interest.

ACKNOWLEDGMENTS

The authors would like to thank Shell Global Solutions (UK) and in particular Roger Cracknell, Trevor Davies and Harold Walmsley for fuel supplies and technical support on fuel properties and evaporation of single and multi-component formulations. Dave Richardson and Steve Richardson at Jaguar Advanced Powertrain Engineering are gratefully acknowledged for technical and financial support. Parts of the work were financially supported by the UK's Engineering and Physical Sciences Research Council (EPSRC).

REFERENCES

1. F. Zhao, M.C. Lai, D.L. Harrington, Automotive spark-ignition direct-injection gasoline engines, Progress in Energy and Combustion Science 25 (1999) 437–562.
2. T. Stach, J. Schlerfer, M. Vorbach, New generation multi-hole injector for direct-injection SI engines, SAE Paper 2007-01-1404, 2007.

3. J. Serras-Pereira, P.G. Aleiferis, D. Richardson, S. Wallace, Mixture formation and combustion variability in a spray-guided DISI engine, SAE Transactions, Journal of Engines 116 (3) (2007) 1332–1356 (Paper 2007-01-4033).
4. J. Serras-Pereira, P.G. Aleiferis, D. Richardson, S. Wallace, Spray development, flow interactions and wall impingement in a DISI engine, SAE Paper 2007-01-2712, 2007.
5. Sarathy, S.M., Thomson, M.J., Togbe, C., Dagaut, P., Halter, F. and Mounaim-Rousselle, C., (2009), "An Experimental and Kinetic Modeling Study of n-Butanol Combustion", Combustion and Flame, Vol. 156, pp. 852–864.
6. Frassoldati, A., Cuoci, A., Faravelli, T., Niemann, U., Ranzi, E., Seiser, R. and Seshadri, K., (2010), "An experimental and kinetic modeling study of n-propanol and iso-propanol combustion", Combustion and Flame, Vol. 157, pp. 2–16.
7. Johnson, M.V., Goldsborough, S.S., Serinyel, Z., O'Toole, P., Larkin, E., O'Malley, G. Curran , H.J., (2009), "A Shock Tube Study of n- and iso-Propanol Ignition", Energy and Fuels, Vol 23, pp. 5886–5898.
8. van Romunde, Z. and Aleiferis, P.G., "Effect of Operating Conditions and Fuel Volatility on Development and Variability of Sprays from Gasoline Direct-Injection Multi-Hole Injectors" Atomization and Sprays, Vol. 19, pp. 207–234, 2009.
9. J. Serras-Pereira, Z. van Romunde, P.G. Aleiferis, D. Richardson, S. Wallace, R.F. Cracknell, "Cavitation, primary break-up and flash boiling of gasoline, iso-octane and n-pentane with a real-size optical direct-injection nozzle", Fuel 89 (2010) 2592–2607
10. Aleiferis, P.G., Serras-Pereira, J., Augoye, A., Davies, T.J., Cracknell, R.F. and Richardson, D., "Effect of Fuel Temperature on In-Nozzle Cavitation and Spray Formation of Liquid Hydrocarbons and Alcohols from a Real-Size Optical Injector for Direct-Injection Spark-Ignition Engines", International Journal of Heat and Mass Transfer, Vol. 53, pp. 4588–4606, 2010.
11. Gu, X., Huang, Z., Li, Q. and Chenglong, T., (2009), "Measurements of Laminar Burning velocities and Markestein Lengths of n-Butanol-air Premixed Mixtures at Elevated Temperatures and Pressures", Energy and Fuels, Vol. 23, pp. 4900–4907.
12. Beeckmann, J., Kruse, S. and Peters, N., (2010), ''Effect of Ethanol and n-Butanol on Standard Gasoline regarding Laminar Burning Velocities'', SAE Paper 2010-01-1452.
13. Beeckmann, J., Rohl, O. and Peters, N., (2009), ''Numerical and Experimental Investigation of Laminar Burning Velocities of iso-Octane, Ethanol and n-Butanol'', SAE Paper 2009-01-2784.
14. Gu, X., Huang, Z., Wu, S. and Li, Q., (2010), "Laminar Burning Velocities and Flame Instabilities of Butanol Isomer-Air Mixtures", Combustion and Flame, Vol. 157, pp. 2318–2325.
15. C.L. Yaws, Yaws' Handbook of Thermodynamic and Physical Properties of Chemical Compounds, Knovel, 2003.
16. Van Romunde, Z.R., "Factors Affecting the Development of Sprays Produced by Multihole Injectors for Direct-Injection Engine Applications", PhD Thesis, University College London, 2011.
17. H.-E. Albrecht, N. Damaschke, M. Borys, C. Tropea, Laser Doppler and Phase Doppler Measurement Techniques, Springer-Verlag, 2002.

18. Pitcher G., Wigley G., Saffman M [1990] – “Velocity and Drop Size Measurements in Fuel Sprays in a Direct Injection Diesel Engine”. Particles and Particle Systems Characterisation, vol. 7, pp 160 – 168, Wiley InterScience.
19. Pitcher G., Wigley G., Saffman M. [1991] – "Sensitivity of Dropsize Measurements by Phase Doppler Anemometry to Refractive Index Changes in Combusting Fuel Sprays", Applications of Laser Techniques to Fluid Mechanics: 5th International Symposium, Lisbon, Portugal 9-12 July 1990, Eds. R.J. Adrian, D.F.G. Durao, F. Durst, M. Maeda and J.H. Whitelaw, (Springer Verlag, New York, 1991), 227-247.
20. Hirleman E.D., Bachalo W.D., Felton P.G., [1990] –“Liquid Particle Size Measurement Techniques” ASTM International, ISBN-10: 0803114591.
21. F. Zhao, D.L. Harrington, M.-C. Lai, 2002, Automotive Gasoline Direct-Injection Engines, SAE, ISBN: 978-0-7680-0882-1.
22. Serras-Pereira, J., Aleiferis, P. G., Richardson, D., Wallace, S. (2008). Characteristics of Ethanol, Butanol, Iso-Octane and Gasoline Sprays and Combustion from a Multi-Hole Injector in a DISI Engine. SAE International Journal of Fuels and Lubricants, Vol. 1, pp. 893-909, Paper 2008-01-1591.
23. van der Wege B.A., Hochgreb S. [2000] – “Effects of Fuel Volatility and Operating Conditions on Fuel Sprays in DISI Engines: (1) Imaging Investigation,” SAE Paper 2000-01-0535.
24. van der Wege B.A., Hochgreb S. [2000, a] – “Effects of Fuel Volatility and Operating Conditions on Fuel Sprays in DISI Engines: (2) PDPA Investigation,” SAE Paper 2000-01-0536.
25. Wigley G., Mehdi M., Williams M., Pitcher G., Helie J., [2006] – “The Effect of Fuel Properties on Liquid Breakup and Atomisation in GDI Sprays” ICLASS, Kyoto, Japan, ICLASS06-075.
26. Ohnesorge W., [1931] – “Die Bildung von Tropfen an Düsen und die Auflösung flüssiger Strahlen.” Zeitschrift für Angewandtw Mathmatik und Mechanik, Bd. 16, Heft 6, pp 355-358.
27. Reitz, R.D. and Bracco, F.V., [1982] – “Mechanisms of Atomization of a Liquid Jet”, Physics of Fluids, Vol. 25, pp. 1730–42.
28. H. Hiroyasu, M. Arai, Structure of fuel sprays in diesel engines, SAE Paper 900475, 1990.
29. H. Hiroyasu, M. Arai, M. Tabata, Empirical equations for the Sauter mean diameter of a diesel spray, SAE Paper 890464, 1989.

LIST OF TABLES

LIST OF FIGURES

Table 1. Selected Fuel Properties.

Fuel Properties	Gasoline	*iso*-Octane	*n*-Pentane	*n*-Butanol	Ethanol	*o*-Xylene
Density [kg/m^3] (20 °C)	719	692	626	809	794	876
Viscosity [cP] (20 °C)	0.3–0.8	0.5	0.2	3.0	1.1	8.1
Surface Tension [mN/m] (20 °C)	25.8	14.7	15.82	25.4	22.4	29.6
Latent Heat [MJ/kg] (25 °C)	0.364	0.305	0.363	0.430	0.902	0.347
Energy Density [MJ/kg], [MJ/lt]	44, 32	45, 31	48, 30	37, 30	29, 23	42, 38
Boiling Point [°C]	30–190	99.8	36.1	117.2	78.5	144.4
Reid Vapour Pressure [bar]	0.56	0.14	1.08	0.02	0.16	0.17
H:C, O:C	1.92, 0	2.25, 0	2.4, 0	2.5, 0.25	3, 0.5	1.25,0
Refractive Index (25 °C)	1.427	1.388	1.358	1.395	1.362	1.496
RON, MON	95, 85	100, 100	62, 61	96, 78	107, 89	101, 87

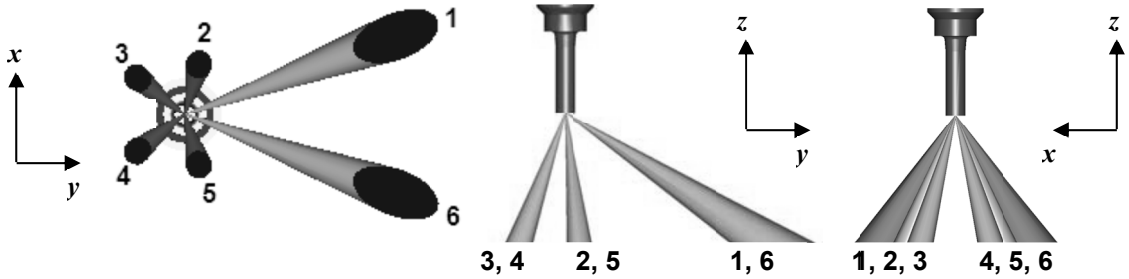

Fig. 1. Schematic of Injector and Spray Plumes.

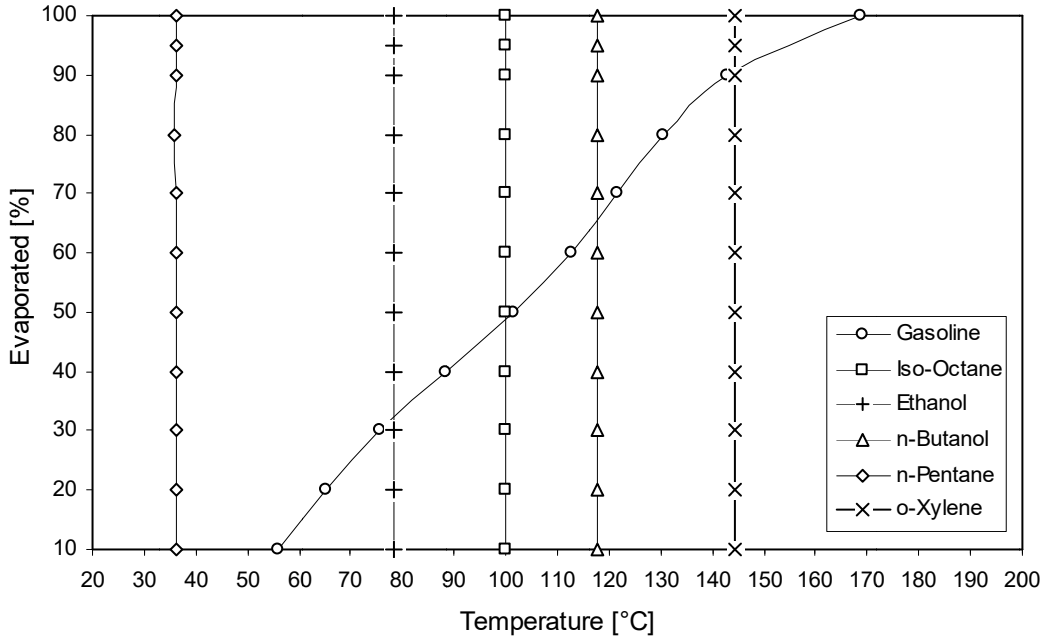

Fig. 2. Distillation Curve of Gasoline Tested and Boiling Points of Single Components.

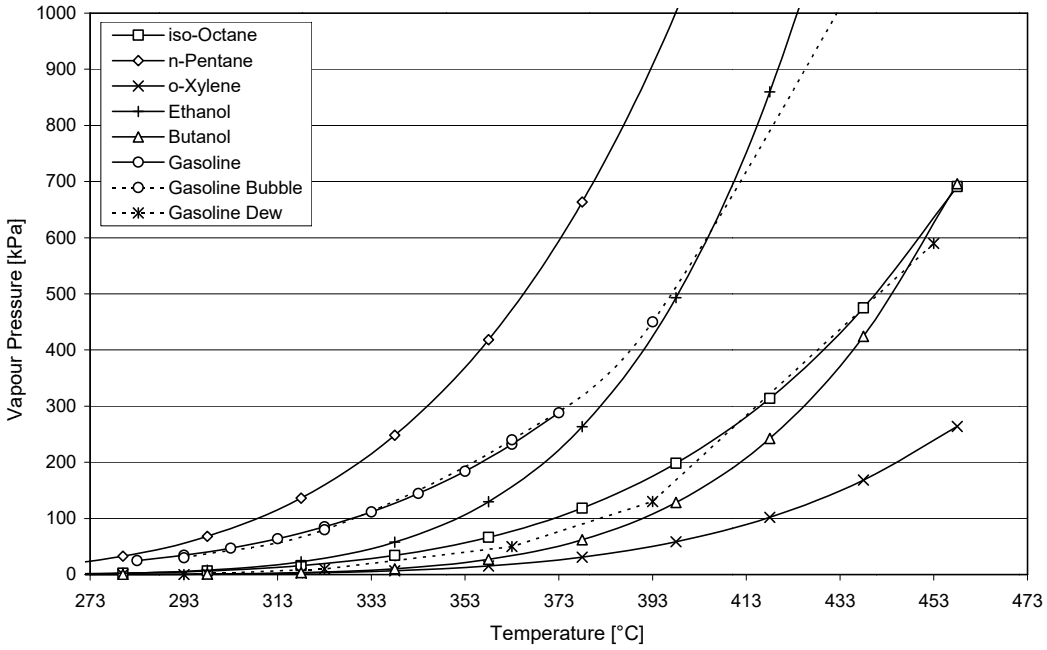

Fig. 3. Vapour Pressure of Fuels.

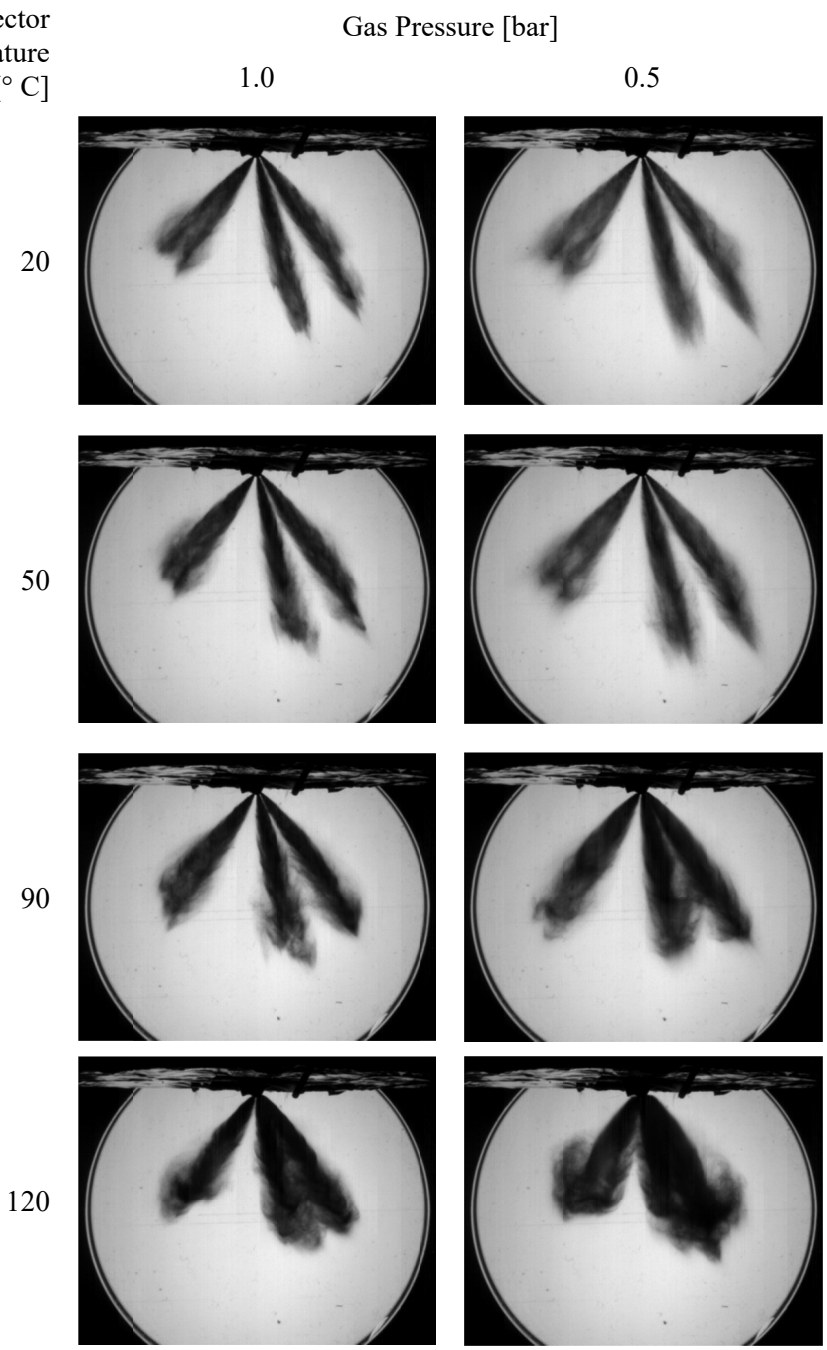

Fig. 4. Ethanol Spray Images, 777 µs ASOI.

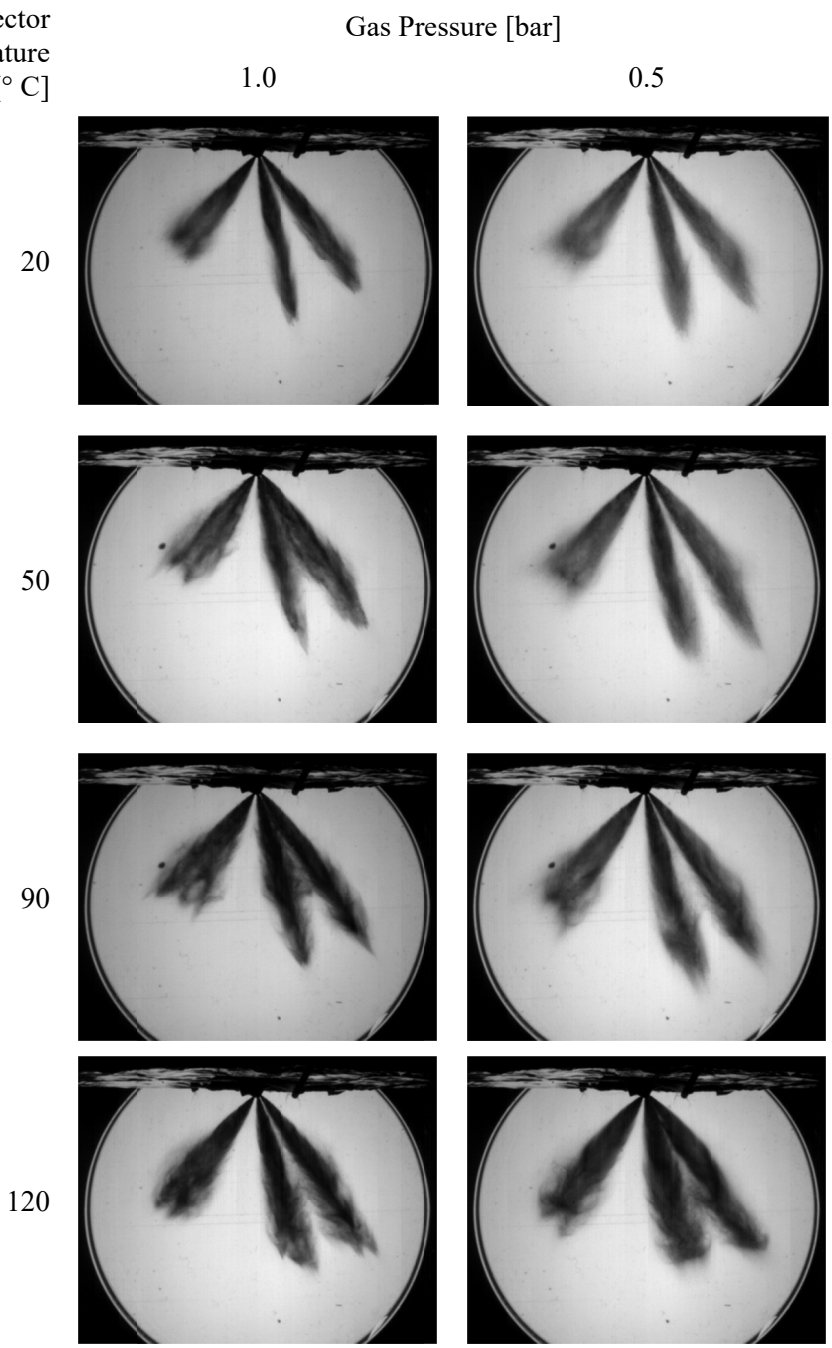

Fig. 5. *n*-Butanol Spray Images, 777 µs ASOI.

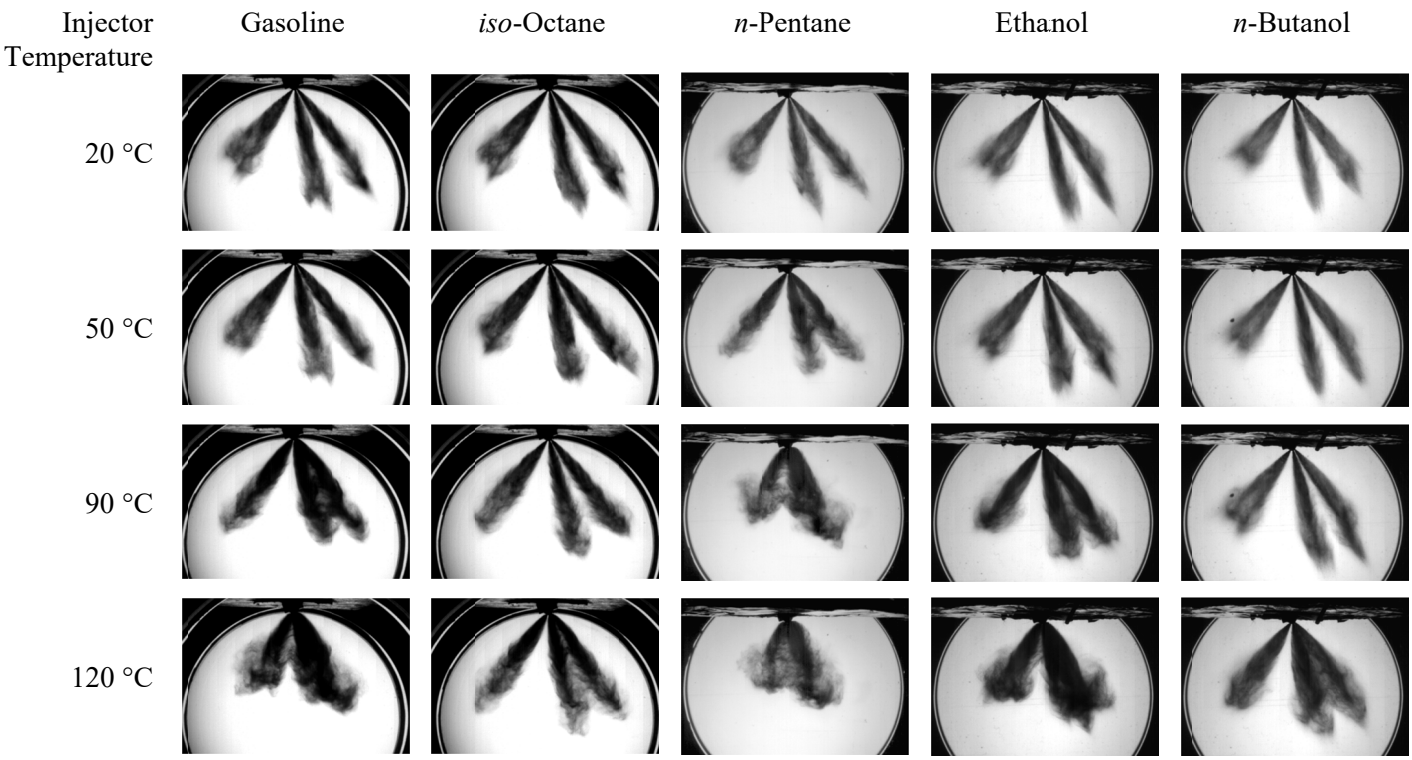

Fig. 6. Spray Images under Range of Temperatures, 0.5 bar, 777 µs ASOI.

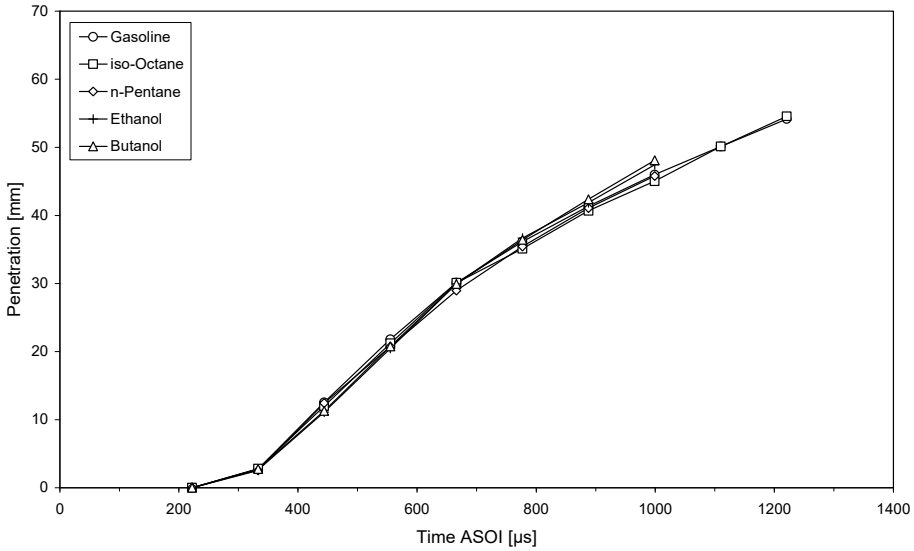

Fig. 7. Plume Penetration, 20 °C, 1.0 bar.

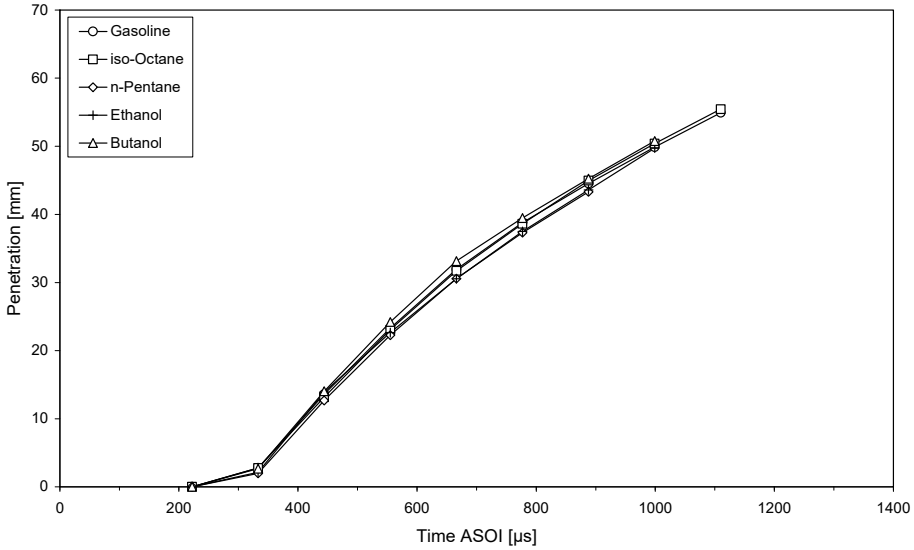

Fig. 8. Plume Penetration, 20 °C, 0.5 bar.

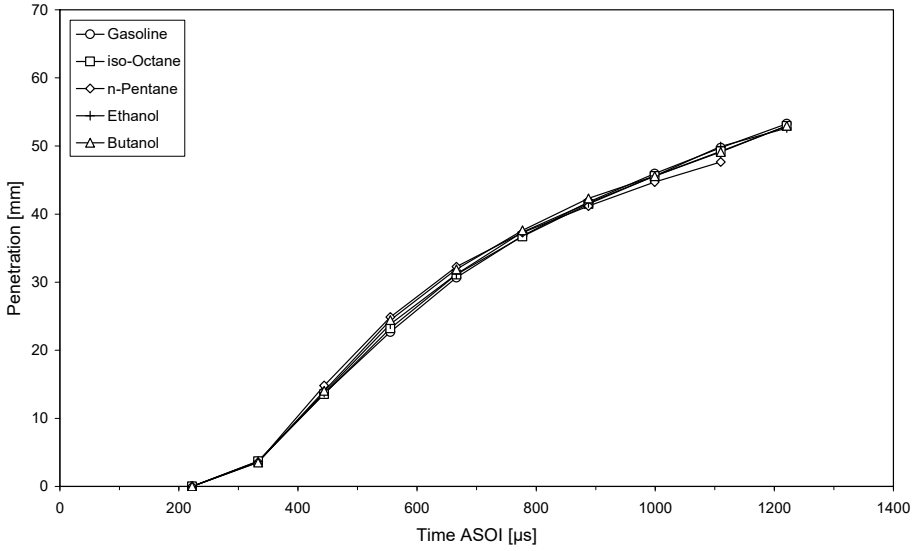

Fig. 9. Plume Penetration, 90°C, 1.0 bar.

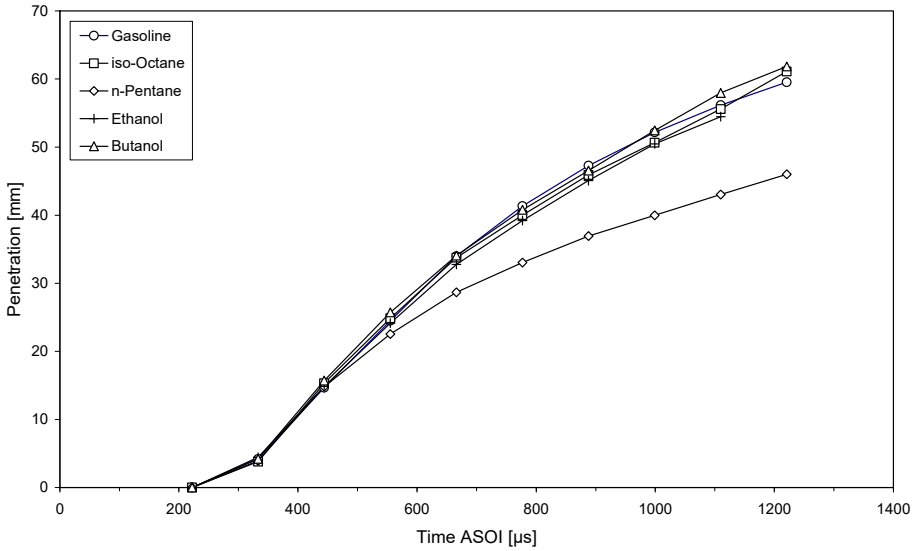

Fig. 10. Plume Penetration, 90 °C, 0.5 bar.

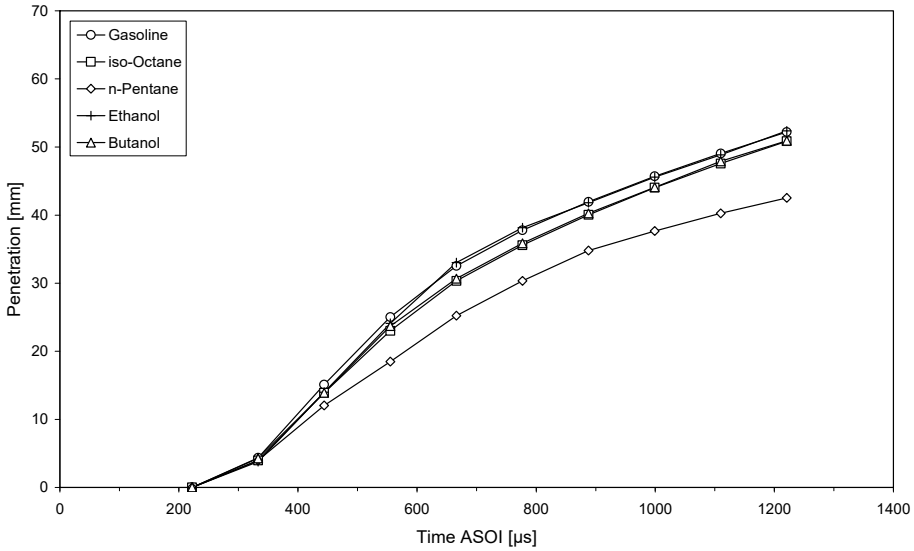

Fig. 11. Plume Penetration, 120°C, 1.0 bar.

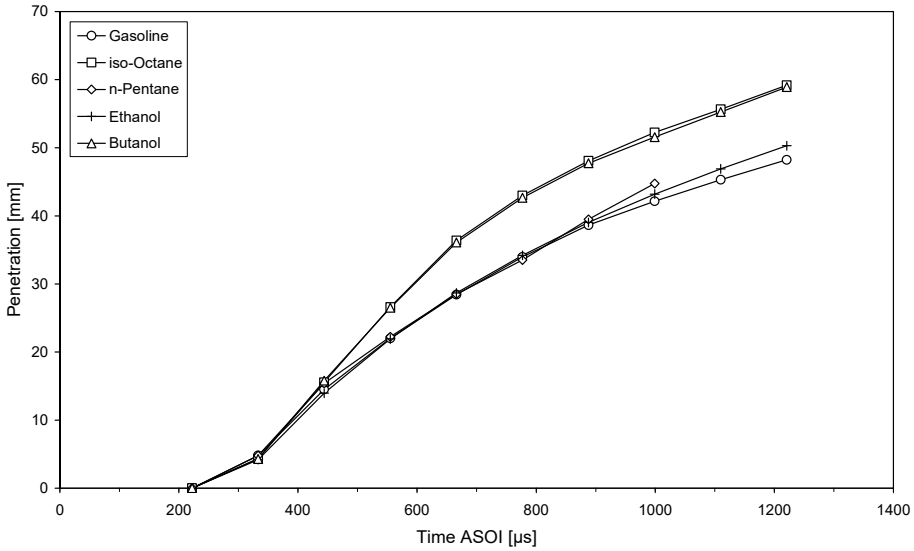

Fig. 12. Plume Penetration, 120 °C, 0.5 bar.

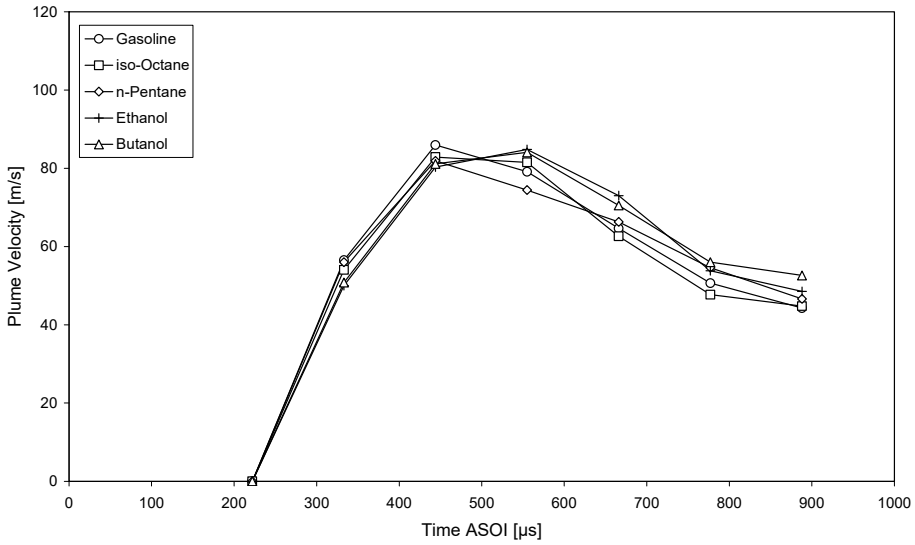

Fig. 13. Spray Tip Velocity, 20 °C, 1.0 bar.

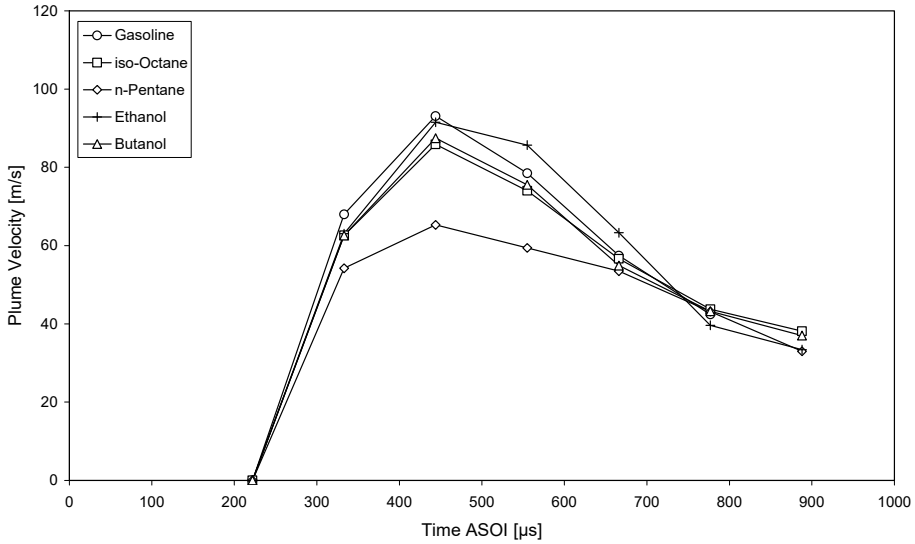

Fig. 14. Spray Tip Velocity, 120 °C, 1.0 bar.

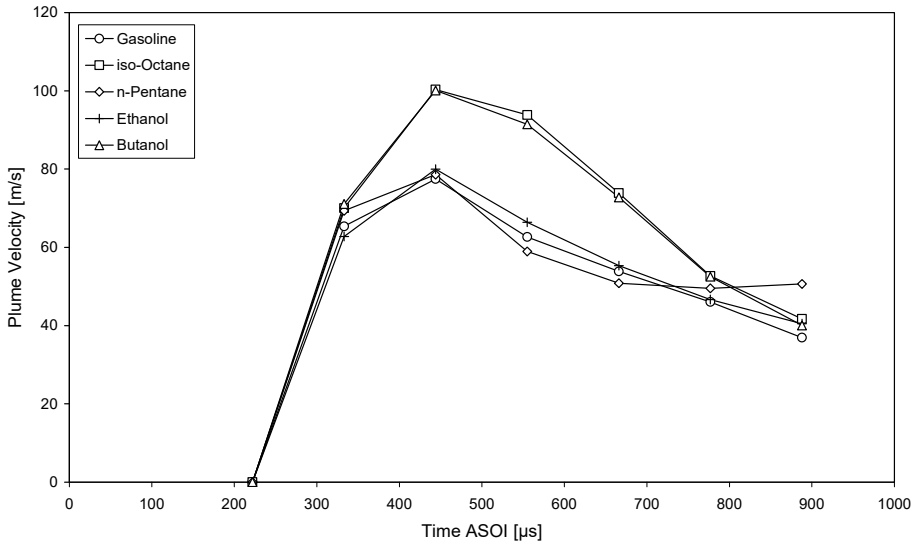

Fig. 15. Spray Tip Velocity, 120 °C, 0.5 bar.

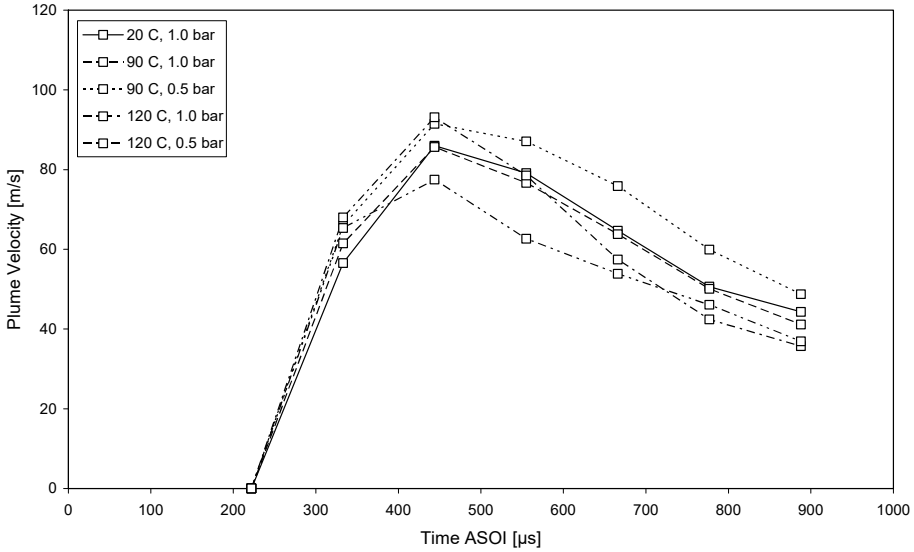

Fig. 16. Spray Tip Velocity, Gasoline.

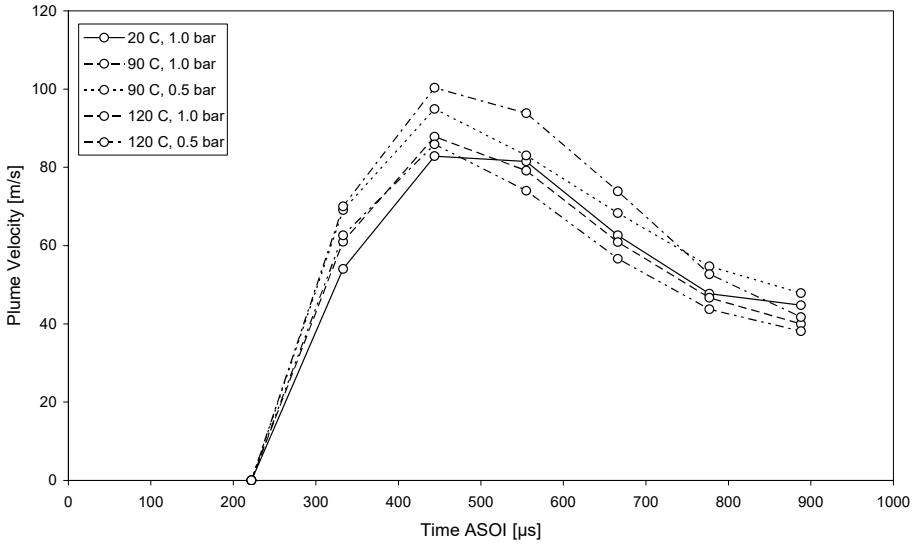

Fig. 17. Spray Tip Velocity, *iso*-Octane.

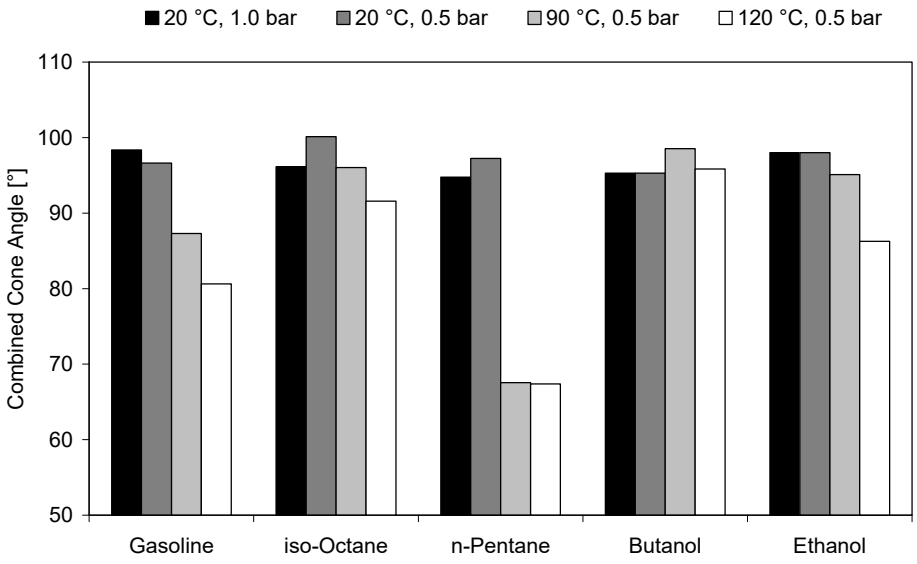

Fig. 18. Spray Cone Angle.

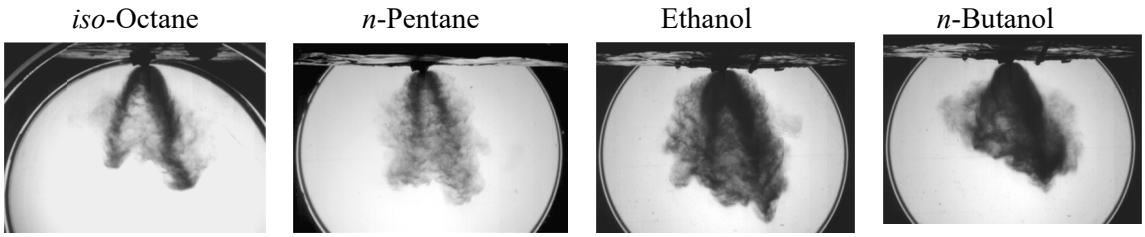

Fig. 19. Spray Images, 180 °C, 0.3 bar, at 777 µs ASOI.

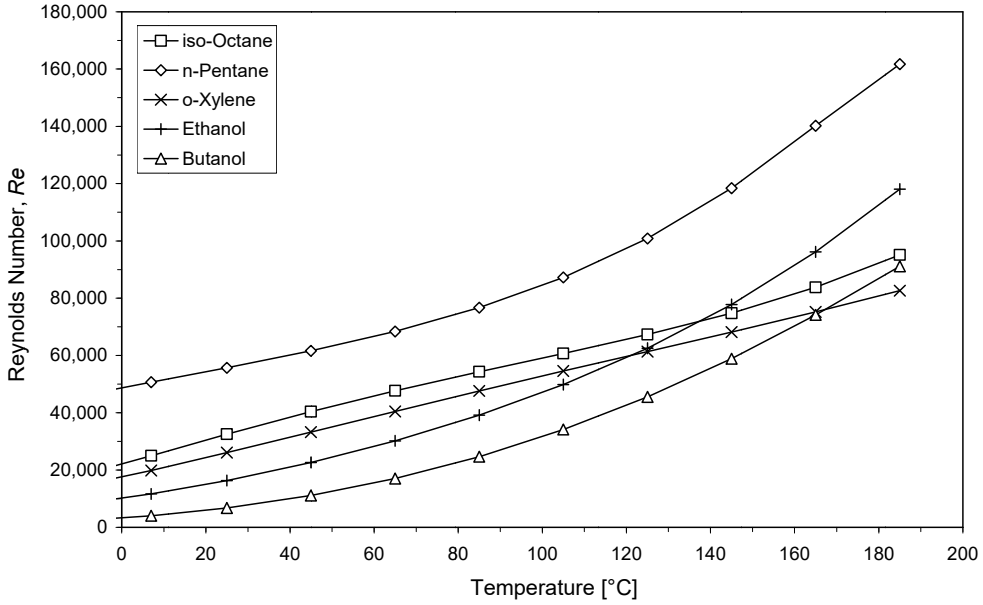

Fig. 20. Reynolds Number.

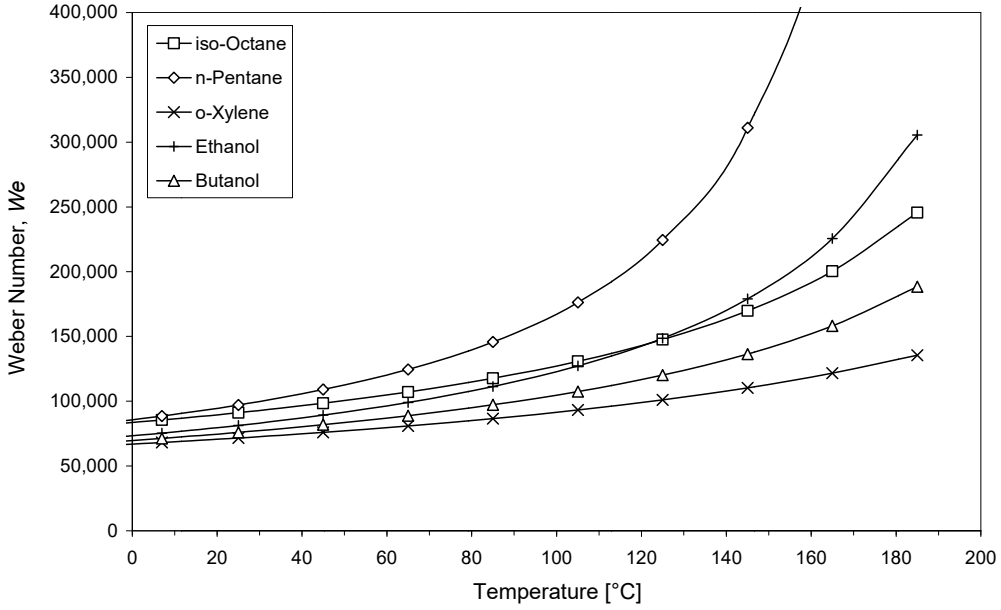

Fig. 21. Weber Number.

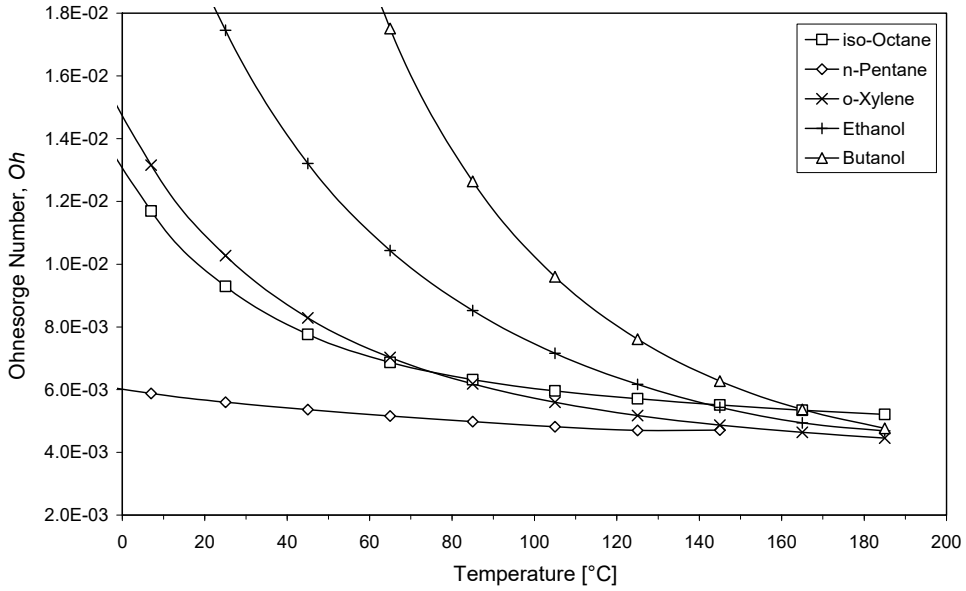

Fig. 22. Ohnesorghe Number.

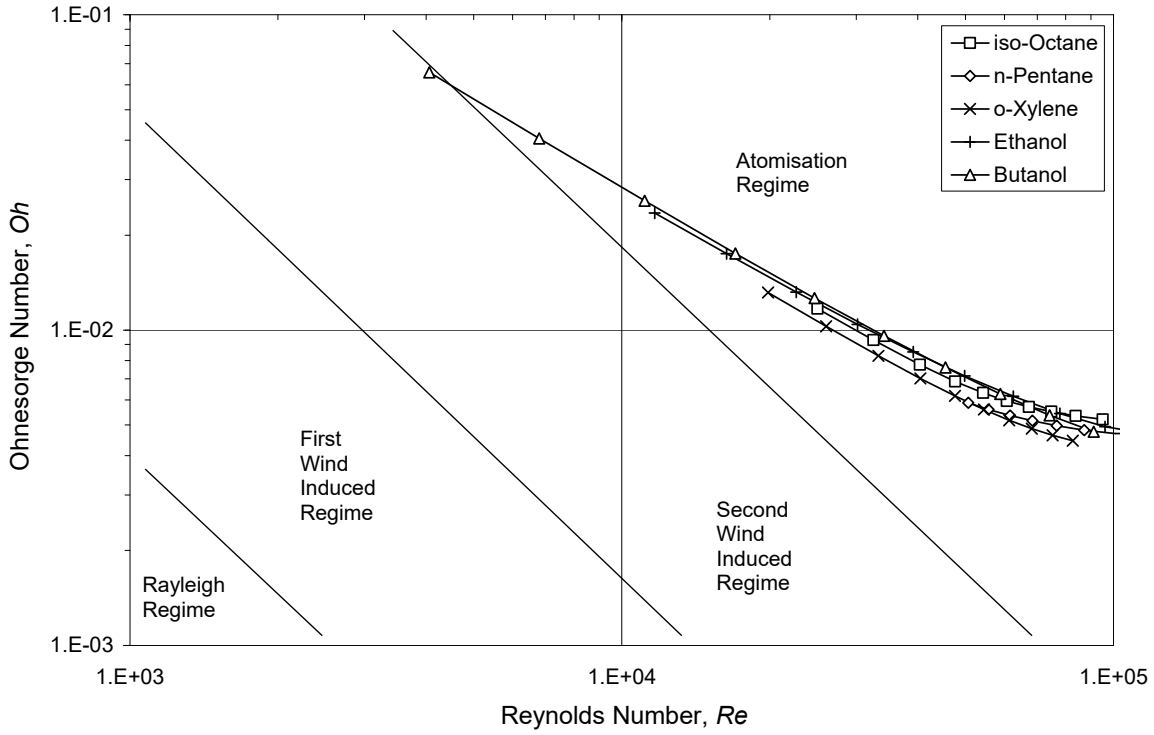

Fig. 23. Ohnesorge Diagram.

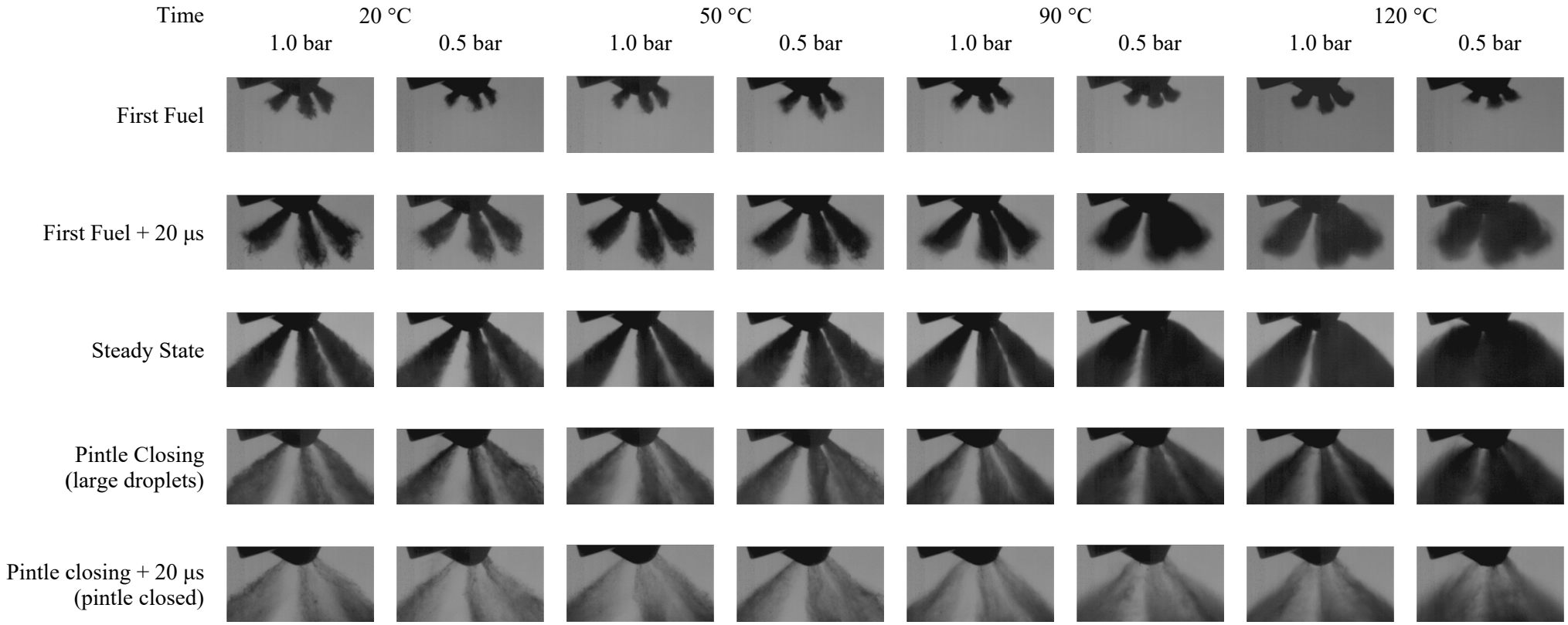

Fig. 24. High-Speed, High-Magnification Spray Imaging, Gasoline.

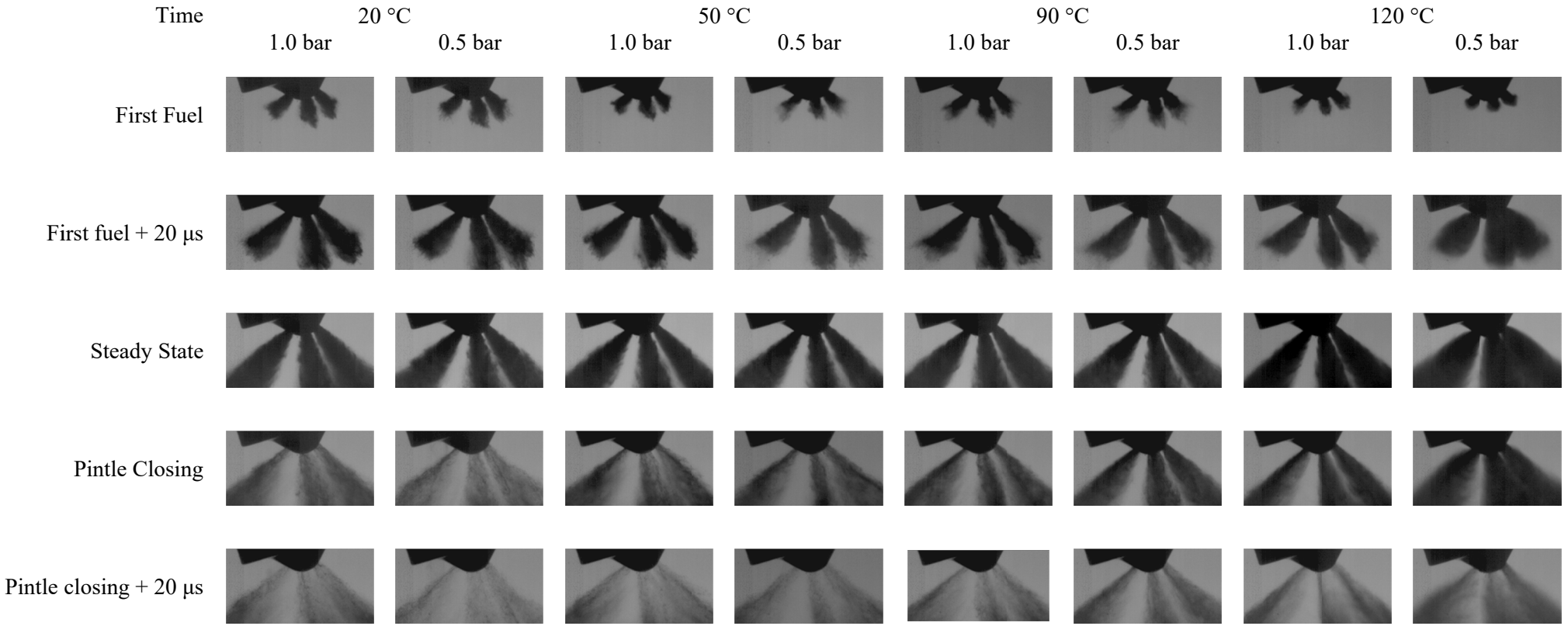

Fig. 25. High-Speed, High-Magnification Spray Imaging, *iso*-Octane.

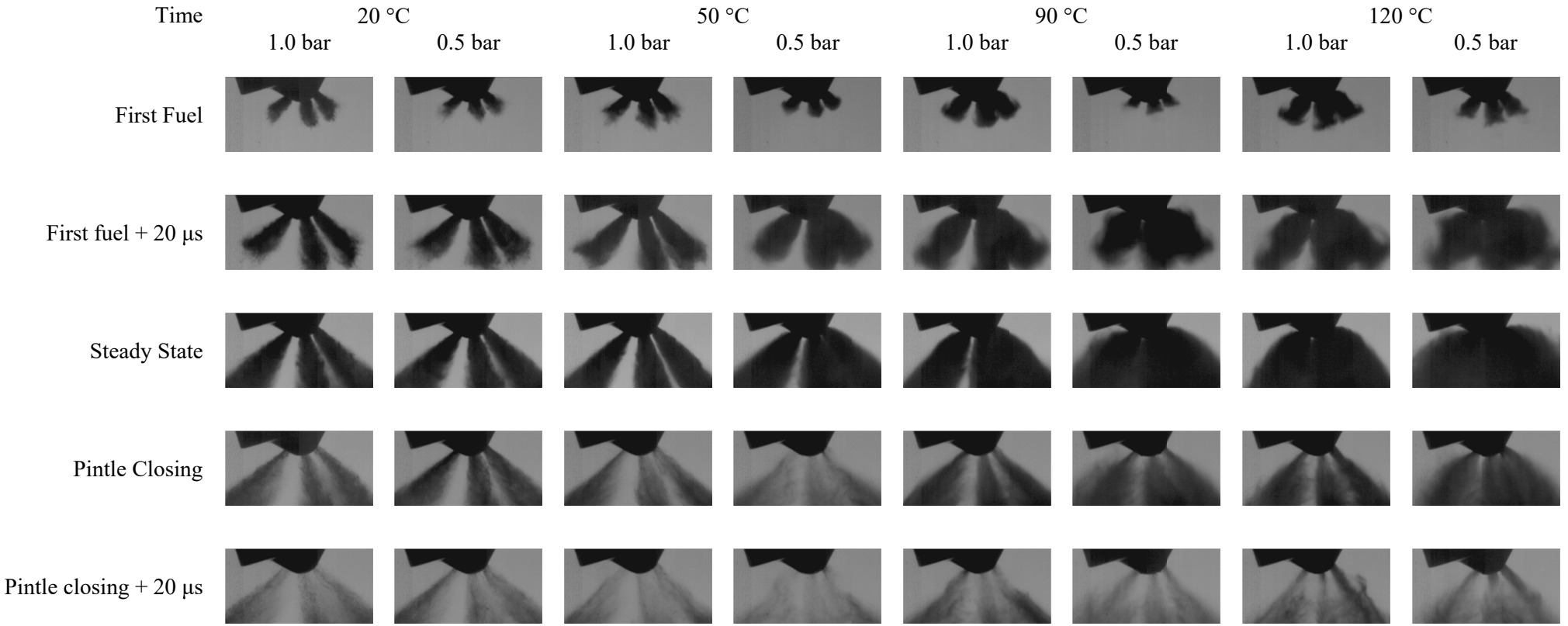

Fig. 26. High-Speed, High-Magnification Spray Imaging, *n*-Pentane.

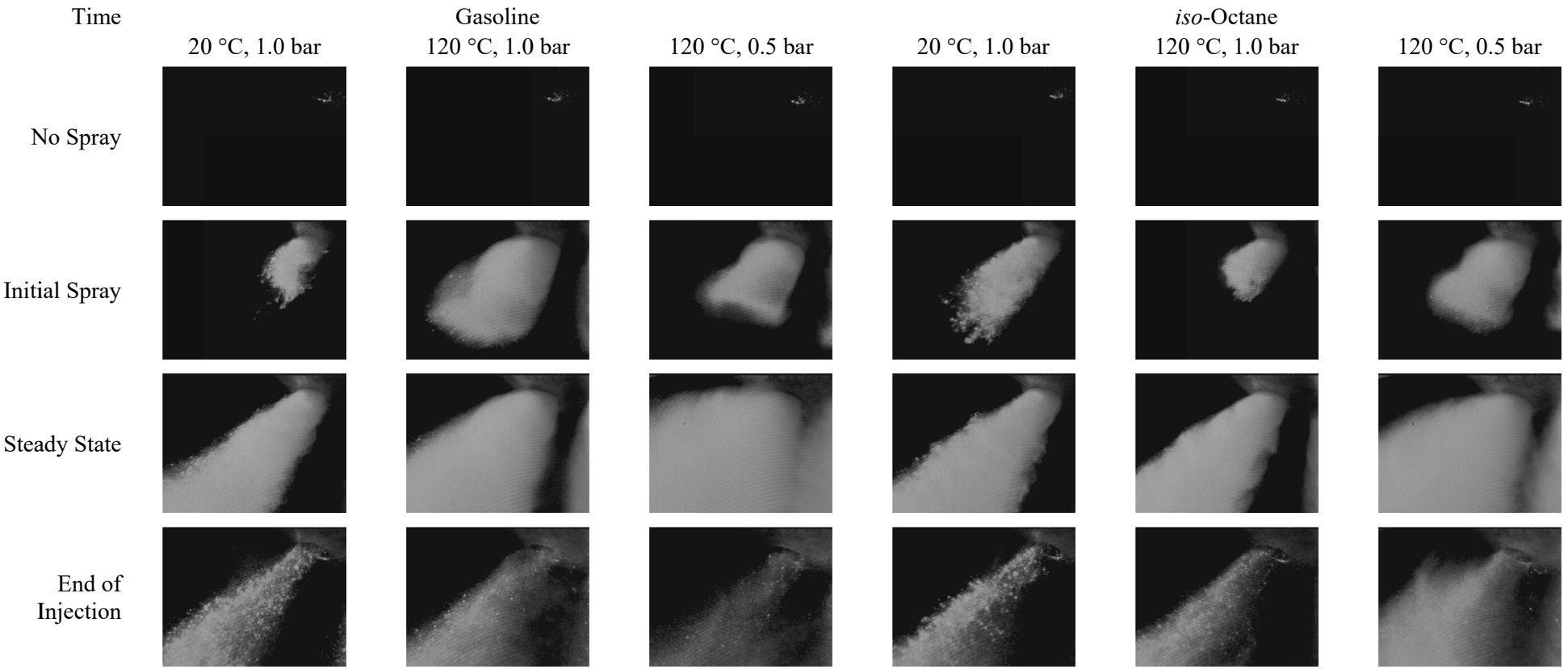

Fig. 27. High-Speed, High-Magnification Spray Imaging, Gasoline and *iso*-Octane (Laser Illumination).

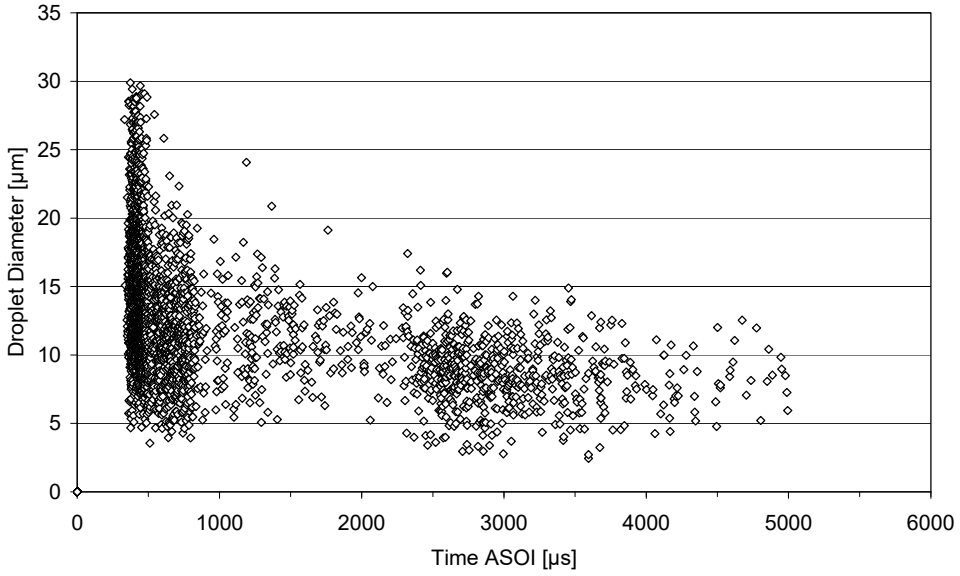

Fig. 28. Spray Droplet Characteristics, Gasoline, 20 °C, 1.0 bar.

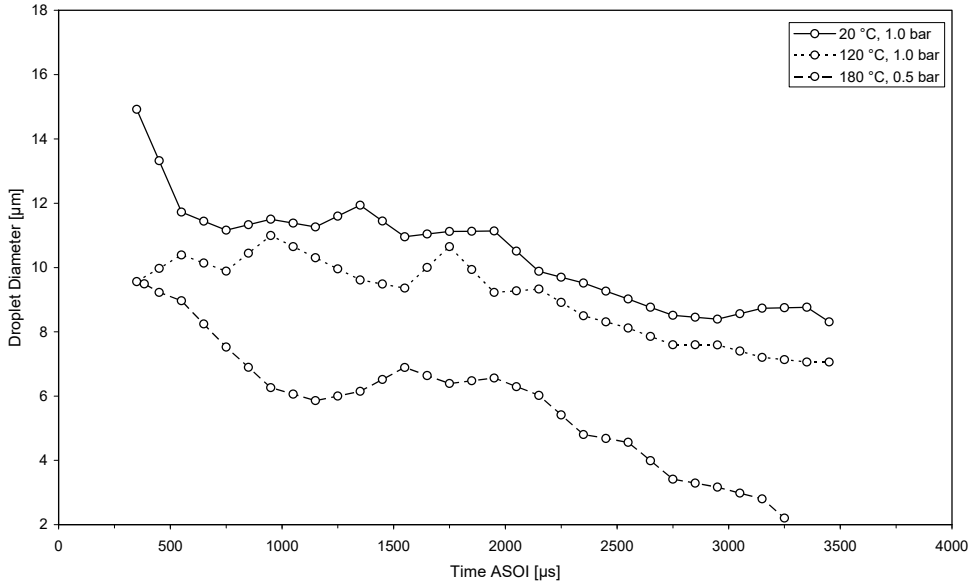

Fig. 29. Droplet Sizes, Gasoline.

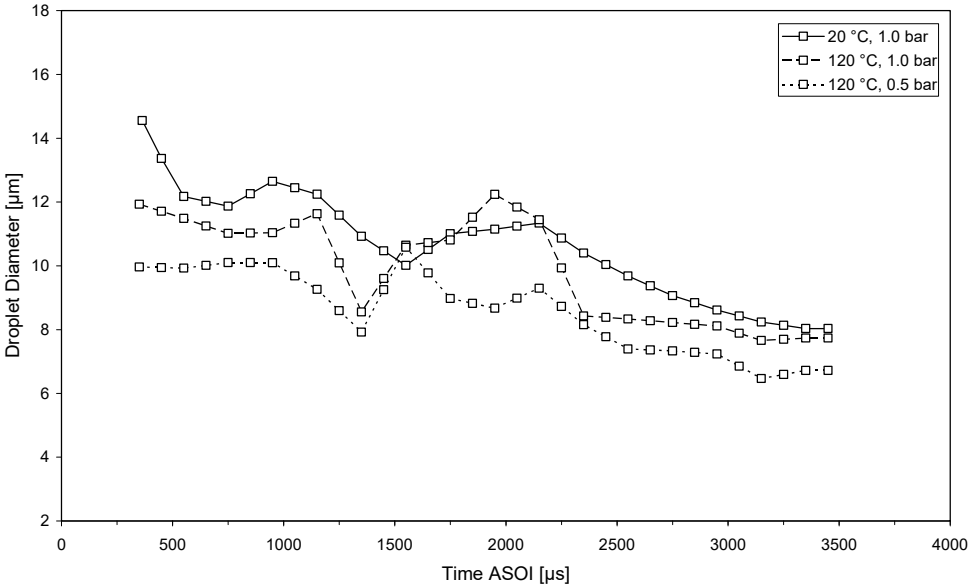

Fig. 30. Droplet Sizes, *iso*-Octane.

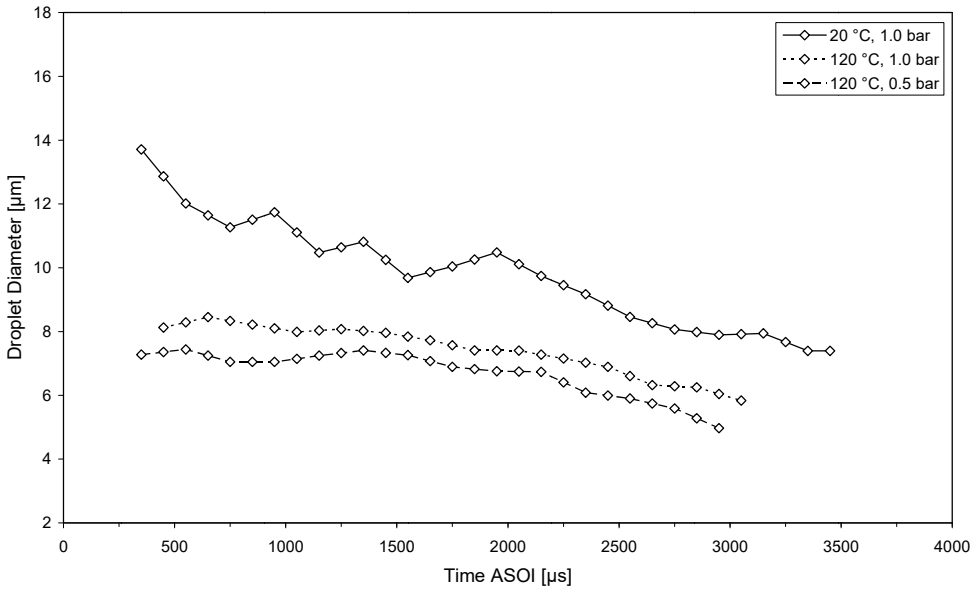

Fig. 31. Droplet Sizes, *n*-Pentane.

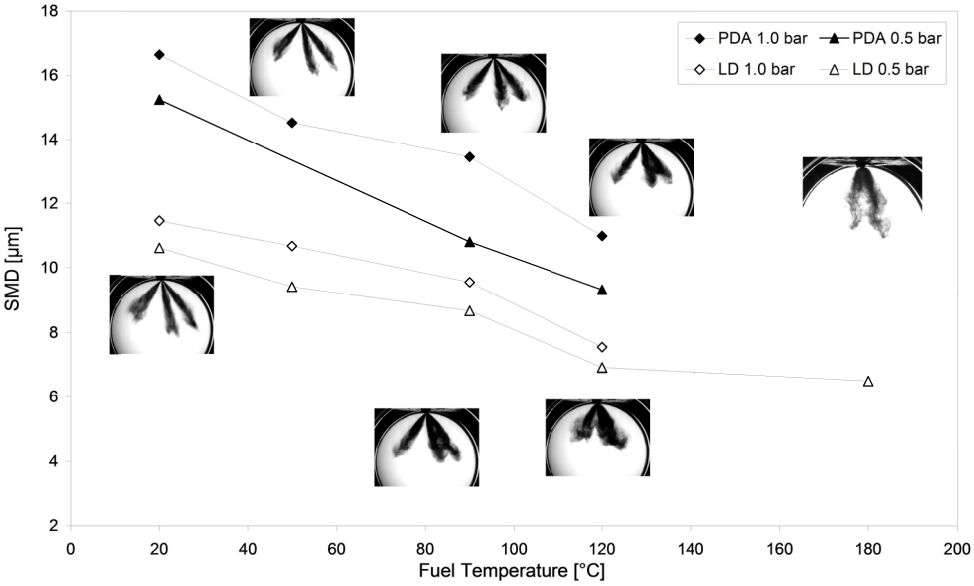

Fig. 32. Sauter Mean Diameter, Gasoline.

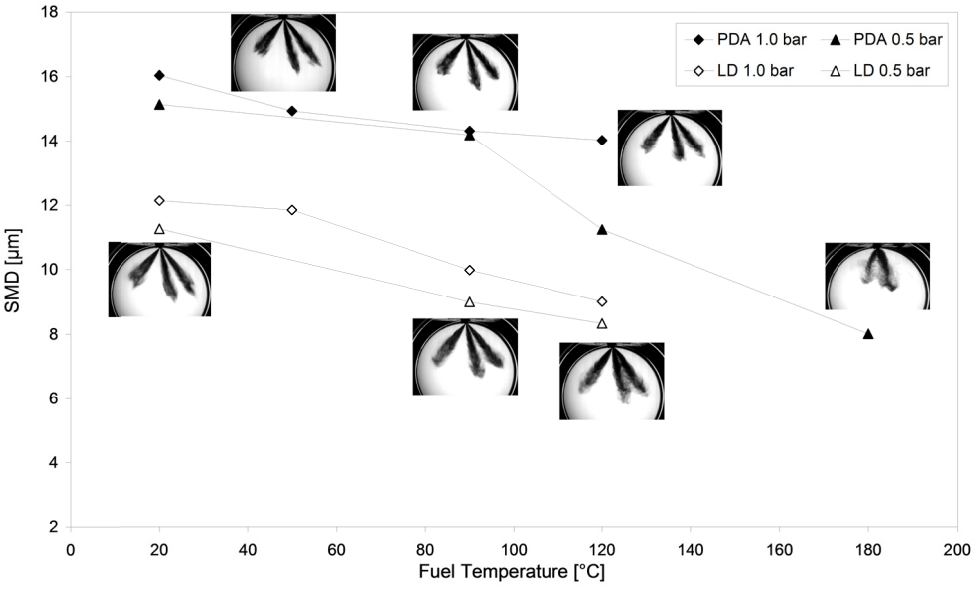

Fig. 33. Sauter Mean Diameter, *iso*-Octane.

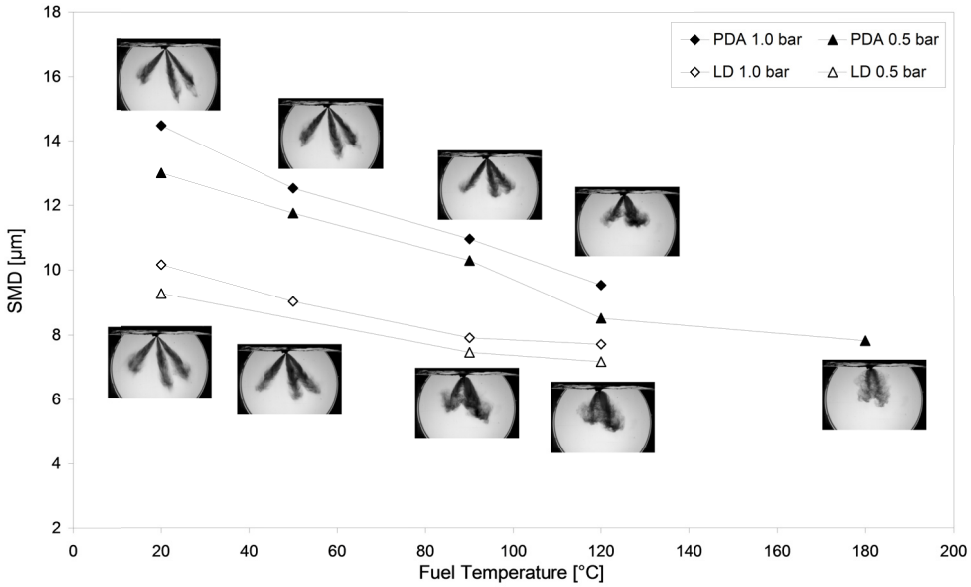

Fig. 34. Sauter Mean Diameter, *n*-Pentane.

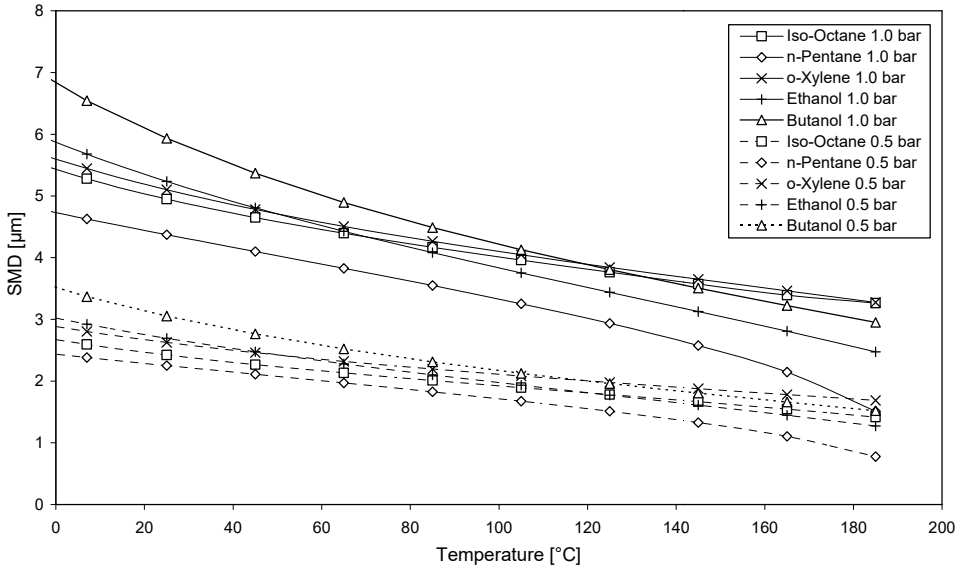

Fig. 35. Calculated Droplet Sizes.

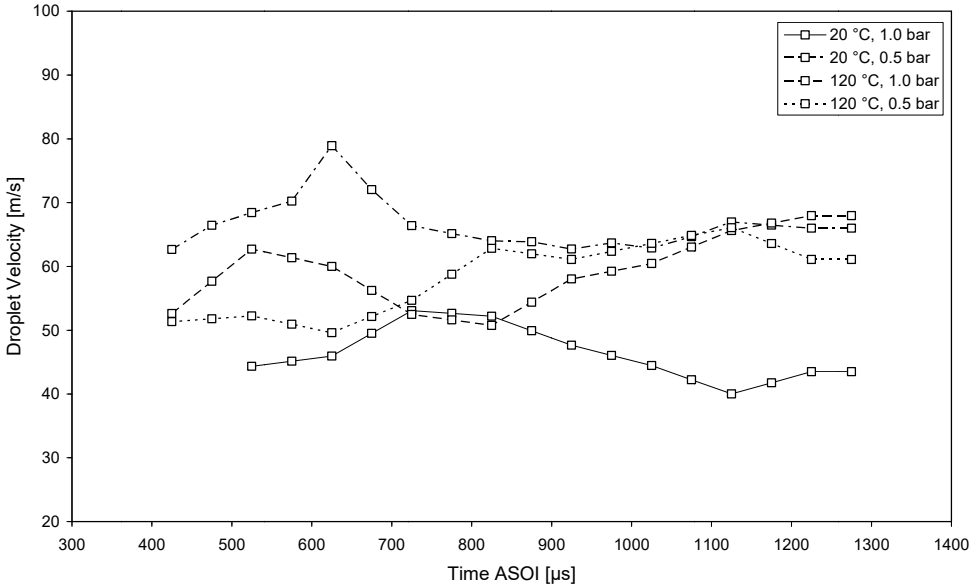

Fig. 36. Droplet Velocities, *iso*-Octane.